

Benjamin HOUANG

**Nanotech
2018**

**Institute for Advanced Biosciences
Centre de Recherche UGA / Inserm U 1209 / CNRS UMR 5309
Site Santé - Allée des Alpes
38700 La Tronche**

Assembly and calibration of bioimaging SWIR platform

from 02/19/18 to 07/08/18



Confidentiality : no

Under the supervision of :

- **Laboratory supervisors : Véronique, JOSSERAND, veronique.josserand@univ-grenoble-alpes.fr & Xavier, LE GUEVEL, xavier.le-guevel@univ-grenoble-alpes.fr**

Present at the defense : yes

- **Phelma Tutor : Marianne, WEIDENHAUPT, marianne.weidenhaupt@grenoble-inp.fr**

**Ecole nationale
supérieure de physique,
électronique, matériaux**

Phelma

Bât. Grenoble INP - Minatec
3 Parvis Louis Néel - CS 50257
F-38016 Grenoble Cedex 01

Tél +33 (0)4 56 52 91 00
Fax +33 (0)4 56 52 91 03

<http://phelma.grenoble-inp.fr>

Acknowledgments

First I would like to thank my tutors Véronique Josserand and Xavier Le Guével for guiding me through my master thesis. They helped me to find solutions and to solve the technical problems during assembly, calibration and experimentation phases of this project. I am also grateful to them for supporting me in my project to join medical school after graduating from Phelma.

I also extend my warmest thanks to Jean-Luc Coll who gave me the opportunity to join his team “Cancer Target & Experimental Therapeutics (CTET)” at the Institute for Advanced Biosciences. He also helped me to become more familiar with the clinical domain by involving me into projects in collaboration with medical doctors, out of the frame of my internship.

I want to address special thanks to Maxime Henry for helping me with the *in vivo* study.

Thanks to Davina Moodely for providing the Quantum Dots from Peter Reiss lab (CEA/INAC).

Thanks to all the other members of the CTET team who contributes to the pleasant prevailing atmosphere in the lab.

Table of contents

Acknowledgments	3
Glossary	8
Framework	9
Introduction.....	10
1- Assembly of optical bench and SWIR camera	15
1.1. Light source	15
1.2. Optics.....	17
1.3. Camera	20
2- Testing SWIR contrast agents and comparison with NIR imaging systems.....	23
2.1. SWIR probes	23
2.1.1. Metallic particles	23
2.1.2. Organic dyes	24
2.2. SWIR probes in intralipid phantom	24
2.3. SWIR probes under chicken slices	27
2.4. In vivo studies with capillaries.....	28
2.5. Models' comparison	30
3- Discussion	32
4- Protocol for new users of the SWIR platform	33
Conclusion	34
Gantt Chart	35
Budget	36
Bibliography.....	37
Appendix.....	39

Figure 1. Visible, NIR-I and NIR-II optical windows from about 900 to 1700 nm, ⁷	10
Figure 2. Light-tissue interactions resulting from impinging excitation light. The blue arrows are the impinging light. The red arrows are the emitted fluorescent signal to detect from the fluorophore symbolized by the red star. The green stars are scattering points. The brown arrow represents autofluorescence of the tissue emitted by an endogenous (produced by the tissue) fluorophore, ⁶ ..	11
Figure 3. These plots of effective attenuation coefficient (on a log scale) versus wavelength show that absorption and scattering from oxygenated blood, deoxygenated blood, skin and fatty tissue is lowest in either the first or second near-infrared window, ⁹	11
Figure 4. Reduced scattering coefficients of different biological tissues and of intralipid scattering tissue phantom as a function of wavelength in the 400–1,700 nm region, which covers the visible, NIR-I and NIR-II windows (blue, green and red shaded regions, respectively). They all show reduced scattering at longer wavelengths, ⁶	12
Figure 5. NIR-I fluorescence image (top left) and cross-sectional fluorescence intensity profile (bottom left) along red-dashed line of a mouse injected with the SWNT-IRDye-800 conjugates. Gaussian fit to the profile is shown in red dashed curve. NIR-II f fluorescence image (top right) and cross-sectional fluorescence intensity profile (bottom right) along red-dashed line of a mouse injected with the SWNT-IRDye-800 conjugates. Gaussian fit to the profile is shown in red dashed curve, ¹⁰	12
Figure 6. A C57Bl/6 mouse head with hair removed Low-magnification cerebral vascular image taken with a field of view of 25 mm× 20 mm. Cerebral vascular image of the same mouse head zoomed into the left cerebral hemisphere, with a field of view of 8mm×6.4mm. Cerebral vascular image of the same mouse head taken using a microscope objective, with a field of view of 1.7 mm× 1.4 mm. The depth of these in-focus vascular features was determined to be 2.6 mm. Zoomed-in image of a sub-region in f taken by a higher-magnification objective, with a field of view of 0.80 mm× 0.64 mm. Inset: cross-sectional intensity profile (black) and Gaussian fit (red) along the yellow-dashed bar, ¹¹ ..	13
Figure 7. High-resolution, high-speed SWIR intravital imaging to generate flow maps of microvascular networks using QD composite particles. a–d, Applying a multi-pass particle image velocimetry approach to the images of the tumour margin (a) and healthy hemisphere (b) generated a flow map for each slice (c, d); coloured arrows indicate the direction and velocity of flow. Scale bars are 300 μ m, ¹²	13
Figure 8. Fluobeam®	13
Figure 9. SWIR platform and LEDs excitation ring.....	14
Figure 10. Industrial design of a) the SWIR platform and b) the excitation ring.....	15
Figure 11. a) 720 nm and b) 810 nm LEDs spectra.	15
Figure 12. a) Gardasoft RT-260-Controller and b) its interface.....	16
Figure 13. Tilting system of the LEDs.....	16
Figure 14. a) Illumination patch on the work plan. b),c) Intensity profiles along diameters of the circular excitation patch on the work plan. The left graph is for λ_{exc} 720 nm. The right one is for λ_{exc} 810 nm.....	17
Figure 15. Principle of the optical bench.....	18
Figure 16. 1000 nm short pass transmission.....	18
Figure 17. Transmission spectra of the a) LP 850 nm, b) LP 1000 nm and c) LP 1300 nm. LP 850 nm has a coating performance OD>2.0 whereas LP 1000 nm and 1300 nm have ODs>4.0 which is for high blocking performances.....	19
Figure 18. Navitar SWIR lens.	20

Figure 19. Princeton Instruments: NIRvana 640ST.....	20
Figure 20. Quantum efficiency of the NIRvana 640ST's InGaAs chip versus wavelength.	20
Figure 21. Lightfield interface.	21
Figure 22. a) Series of Au NCs : AuPeg600NH ₂ , AuZwMe ₂ , AuMHA/EDT and their fluorescence emission profiles (1 mg Au/mL in water, λ_{exc} 450nm). b) Fluorescence emission of QDs at each synthesis step (0.1 mg /mL in hexane, λ_{exc} 450nm). c) ICG and IR800 formula and fluorescence emission spectra (0.1 mg /mL in PBS, λ_{exc} 700nm).....	23
Figure 23. Protocol of phantom synthesis from left to right: solution preparation, agarose dissolution on hot plate and molding.	24
Figure 24. a) Intralipid phantom schematic under LED excitation showing the different depths at which the SWIR probes were tested. b) Picture of the experiment.	25
Figure 25. 1% intralipid phantom autofluorescence measured on SWIR platform with LP 1000 nm and 1300 nm filters, 200 ms exposure time: a) λ_{exc} 720 nm b) λ_{exc} 810 nm.....	25
Figure 26. Normalized fluorescence intensity of AuMHA/EDT (1 mg Au/mL) versus depth in 1% intralipid phantom: a) Fluobeam®800, λ_{exc} 780 nm, 100 ms exposure time for LP 830 nm, b) SWIR platform, λ_{exc} 720 nm, 10 ms exposure time for LP 1000 nm, 200 ms exposure time for LP 1300 nm, c) SWIR platform, λ_{exc} 810 nm, 10 ms exposure time for LP 1000 nm, 200 ms exposure time for LP 1300 nm.....	26
Figure 27. Signal to Noise Ratio of IR 800 versus depth on SWIR platform, λ_{exc} 720 nm, LP 1000 at 50, 100 and 200 ms exposure times.	27
Figure 28. AuMHA/EDT (1mgAu/mL) capillary under excitation (left). Chicken slice staking over the capillary (middle and right).	27
Figure 29. Normalized fluorescence intensity of AuMHA/EDT (1 mg Au/mL) versus depth under chicken slices: a) Fluobeam®800, λ_{exc} 780 nm, 100 ms exposure time for LP 830 nm, b) SWIR platform, λ_{exc} 720 nm, 10 ms exposure time for LP 1000 nm, 200 ms exposure time for LP 1300 nm, c) SWIR platform, λ_{exc} 810 nm, 10 ms exposure time for LP 1000 nm, 200 ms exposure time for LP 1300 nm.	28
Figure 30. Nude mouse skin autofluorescence measured on SWIR platform with a) LP 1000 nm and b) 1300 nm filters, 200 ms exposure time, λ_{exc} 810 nm. c) Signal to noise ratio of autofluorescence on background.....	29
Figure 31. a) Subcutaneous capillary experiment. b)-e) AuPEG1000NH ₂ , AuZwMe ₂ , AuMHA/EDT 1.5/0.5, 2.5 mg Au/mL and ICG 0.1 mg/mL subcutaneous capillaries in mice, LP 1300 nm, 200 ms exposure time, λ_{exc} 810 nm. Signal to Noise Ratio of the previously described (b)-e))contrast agents f) under LP 1000 nm, g) under LP 1300 nm.	29
Figure 32. a) AuMHA-EDT 2,5 mg Au/mL, ventral side intra-rectal, λ_{exc} 810 nm, LP1000nm 10 ms. b) QDs, ventral side intra-rectal, λ_{exc} 810 nm, LP1000nm; 10 ms.	30
Figure 33. Relative fluorescence along a perpendicular cross section of a capillary filled with AuMHA/EDT 0.5/1.5 λ_{exc} 810 nm a) in 1% intralipid phantom 6mm deep, b) under chicken 2 mm deep, c) as subcutaneous implant in mouse depth < 1mm.	31
Figure 34. Normalized fluorescence intensity of ICG versus depth: a) Fluobeam®800, λ_{exc} 780 nm, 500 ms exposure time for LP 830 nm, b) SWIR platform, λ_{exc} 720 nm, 100 ms exposure time for LP 1000 nm, 1s exposure time for LP 1300 nm, c) SWIR platform, λ_{exc} 810 nm, 100 ms exposure time for LP 1000 nm, not detectable (*) for LP 1300 nm.	40
Figure 35. Normalized fluorescence intensity of IR 800 versus depth: a) Fluobeam®800, λ_{exc} 780 nm, 5 ms exposure time for LP 830 nm, b) SWIR platform, λ_{exc} 720 nm, 50 ms exposure time for LP 1000 nm, 1s exposure time for LP 1300 nm.....	40

Table 1. Comparison between Fluobeam® 800 and NIRvana 640 ST.....	22
---	----

Glossary

- A/D converter : Analog to Digital converter
- CHU : University Hospital Center
- CNRS : Centre National de la Recherche Scientifique
- CTET: Cancer Target & Experimental Therapeutics
- FDA : Food and Drug Administration
- IAB : Institute for Advanced Biosciences
- Inserm : Institut National de la Santé Et de la Recherche Médicale
- LED : Light-Emitting Diode
- LOD : Limit Of Detection
- LP : Long Pass
- NA : Not Available
- NIR : Near InfraRed
- NP : Nanoparticle
- OD : Optical density
- PBS : Phosphate Buffered Saline solution
- QD : Quantum dot
- SNR : Signal to Noise Ratio
- SWIR : ShortWave InfraRed
- UGA : Université Grenoble Alpes
- 2/3D : 2/3 dimensions

Framework

My internship took place at the Institute for Advanced Biosciences (IAB) located in La Tronche next to the CHU of Grenoble.

This research center, under the trusteeship of UGA, INSERM and CNRS, presents several fields of expertise covering the biological continuum, from the molecule to population, genetics, epigenetics, signalization and chromatin, cell-biology, cellular-matrix interactions, molecular pathologies, host-parasites interactions, immunology and environmental epidemiology.

Its three main axes of investigation are the following:

1. Understand the mechanisms leading epigenetic modifications to the development of normal and pathologic phenotypes by coordinating the genome dynamic with the environmental signals and constraints.
2. Innovate in cancer detection, diagnostic and treatment by targeting the mechanisms and the way the genome “communicates” with the cellular and extra-cellular environment.
3. Understand how chronic pathologies and cancers appear and progress in their genetic, epigenetic and environmental context, and contribute to the development of new relevant concepts in terms of public health and patient care improvement.

IAB hosts several technical platforms such as optical microscopy/ cellular imaging (MicroCell), flux cytometry, optical imaging of small animals (OPTIMAL), and bioinformatics for fundamental and medical epigenetics (EpiMed).

I worked within the team “Cancer Target & Experimental Therapeutics (CTET)” led by Jean-Luc Coll. The team is evolving in a dynamic transdisciplinary environment where biologists, chemists, engineers, biotech companies and medical doctors are working together.

One of the fields of their expertise relies on the development of new delivery systems in the nanometric size with specific design enabling early cancer diagnosis, *in vivo* optical imaging and targeted therapy. For example, several types of nanoparticles with controlled surface chemistry and emitting in the near infrared region have been extensively studied in the lab in different cancer models ¹. These new compounds are tested *in vitro* in 2D, 3D cell-culture models and *in vivo* in mice models with optical instruments to demonstrate their therapeutic and/or diagnostic activities for multimodal imaging, targeted drug delivery, but also radiosensitization and phototherapy ². The OPTIMAL platform for small animal optical imaging, which is part of the lab, is thus evaluating new contrast agents and theranostic (therapy+diagnostic) systems from the group and from collaborators to characterize their toxicity, *in vivo* biodistribution and therapeutic efficacy against cancer.

In parallel the team is developing new optical imaging devices that are intended to be transferred to the clinical domain in particular for guided surgery. For instance, they can be used in plastic surgery to identify and monitor flaps’ perfusion ³. Fluorescence imaging also enables to visualize the lymphatic network, thus helping to detect the sentinel lymph node ⁴. Eventually, endocrinal surgery takes profit from this technology to identify parathyroid glands and avoid their resection during thyroidectomy ⁵.

Introduction

Biomedical imaging has become an essential tool for physicians enabling more precise diagnosis thanks to the anatomical, physiological and pathological information it can provide in addition to the clinical exam ⁶.

Conventional clinical imaging modalities (x ray scanner, MRI, PET/SPECT, ultrasound) are mostly used for diagnosis and to follow disease evolution and therapeutic efficacy. More recently imaging is also entering in the surgery room to guide the surgeon and to help decision making in real time.

The visible (400-700 nm) and the first infrared NIR-I (700-850 nm) windows (Figure 1) ⁷ are also exploited for optical imaging in the medical domain and more precisely in guided surgery ³⁻⁶. In comparison with tomographic imaging technics, *in vivo* fluorescence imaging provides a wide field image acquisition in real time with limited diffraction and spatial resolution thanks to non-hazardous interactions of the optical radiations with the tissues or contrast agents. The light-matter interactions on which is based this technic are described in Figure 2 ⁶. An excitation light (blue arrows) is sent towards the area of interest and penetrates the tissue. During their travel, the photons encounter scattering points (green crosses) and absorbing elements (purple cross) until they reach the contrast agent (red star) or endogenous fluorophores that generate tissue autofluorescence (brown arrow). The excited fluorophore (endogenous or exogenous) starts emitting photons of lower energy and thus longer wavelength than the excitation which travel out and are detected with an infrared detector ⁸. Working in the NIR-I window instead of in the visible region enable a deeper light penetration in tissues and thus increases the detection sensitivity necessary to image the organs ⁶. Despite these advances, the penetration depth of light through the skin and biological tissues does not exceed few millimeters and the weak emission signal related to the heterogeneity of tissues and the absorption of natural elements such as hemoglobin (Figure 2, Figure 3) ^{6,9} is still limited both the sensitivity and the resolution.

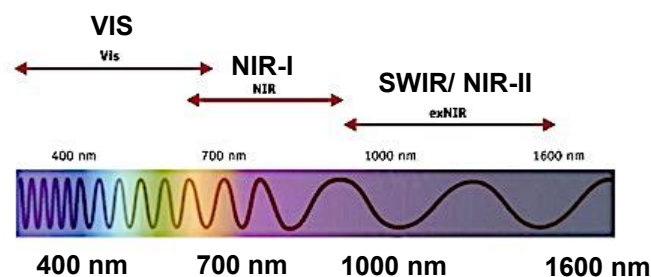


Figure 1. Visible, NIR-I and NIR-II optical windows from about 900 to 1700 nm, ⁷.

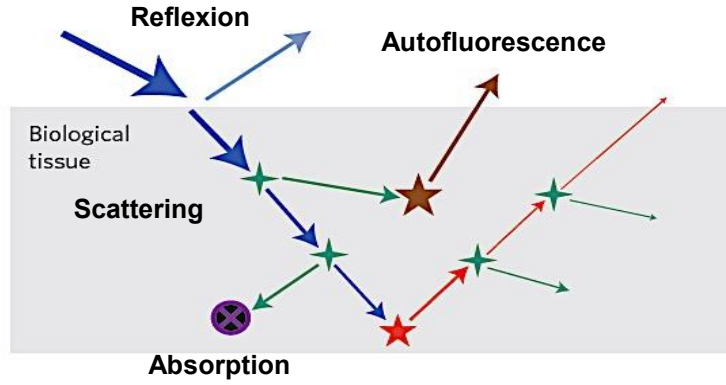


Figure 2. Light-tissue interactions resulting from impinging excitation light. The blue arrows are the impinging light. The red arrows are the emitted fluorescent signal to detect from the fluorophore symbolized by the red star. The green stars are scattering points. The brown arrow represents autofluorescence of the tissue emitted by an endogenous (produced by the tissue) fluorophore, ⁶.

Recently, several research groups have been investigating the near-infrared spectral window commonly known as SWIR for ShortWave InfraRed or NIR-II between 850 and 1700 nm (Figure 1) for bioimaging ⁷. Despite the development of cameras in this spectral window for military applications (thermal detection), industrial (freshness of food) or artistic (analysis of works of art), their use for biomedical applications remains at their infancy. The SWIR window shows a fall in photon scattering and tissue autofluorescence compared to Vis-NIR-I domains (Figure 4) ⁶. Although there is no significant decrease of blood, fat and skin's absorption coefficients in the 1000-1400 nm of the SWIR region compared to the NIR-I (600-1000 nm) (Figure 3) ⁹, SWIR window offers a strong reduced scattering because for photons a longer wavelength means lower energy which leads to less interaction with the environment, especially for brain tissue, intralipid tissue phantom and skin. This behavior can be read on the scattering coefficient μ_s' evolving like a decaying exponential versus the wavelength (Figure 4) ⁶:

$$\mu_s' \propto \lambda^{-\alpha} \text{ with } 0.2 \leq \alpha \leq 4 \text{ for biological tissues}^6$$

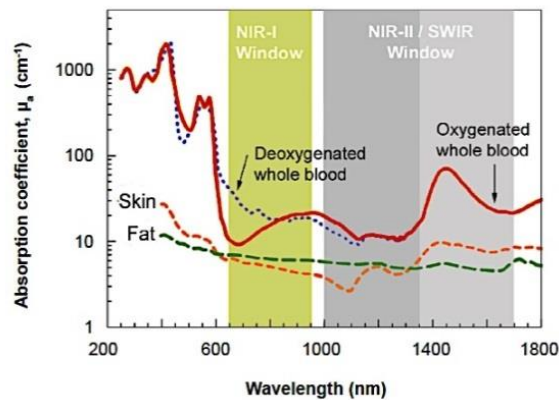


Figure 3. These plots of effective attenuation coefficient (on a log scale) versus wavelength show that absorption and scattering from oxygenated blood, deoxygenated blood, skin and fatty tissue is lowest in either the first or second near-infrared window, ⁹.

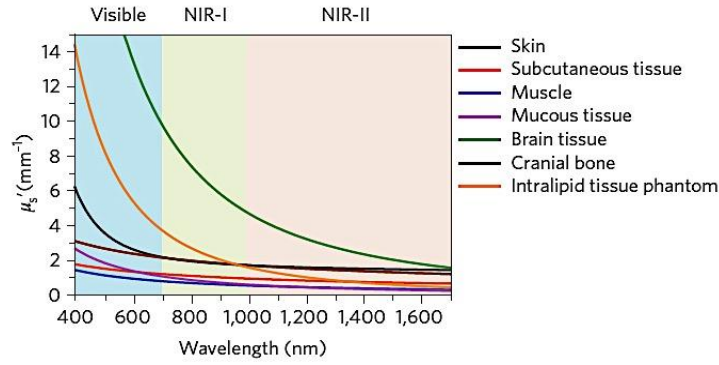


Figure 4. Reduced scattering coefficients of different biological tissues and of intralipid scattering tissue phantom as a function of wavelength in the 400–1,700 nm region, which covers the visible, NIR-I and NIR-II windows (blue, green and red shaded regions, respectively). They all show reduced scattering at longer wavelengths, ⁶.

Two research groups from US are pioneers in the domain of SWIR bio-imaging and have presented very promising results on the use of SWIR imaging to obtain high quality of detection in small animals ^{10–16}.

In Stanford University, Hongjie Dai and his team coupled some carbon nanotubes used as contrast agent in the SWIR region with IR 800 which is an FDA approved fluorophore emitting in the NIR-I range. This way, he was able to simultaneously take images of mice hind limb in both windows and thus demonstrate the improved spatial resolution in the SWIR called NIR-II (Figure 5) ¹⁰. In another study, they performed brain vasculature SWIR imaging still using carbon nanotubes with a resolution going down to 6.6 μm (Figure 6) ¹¹.

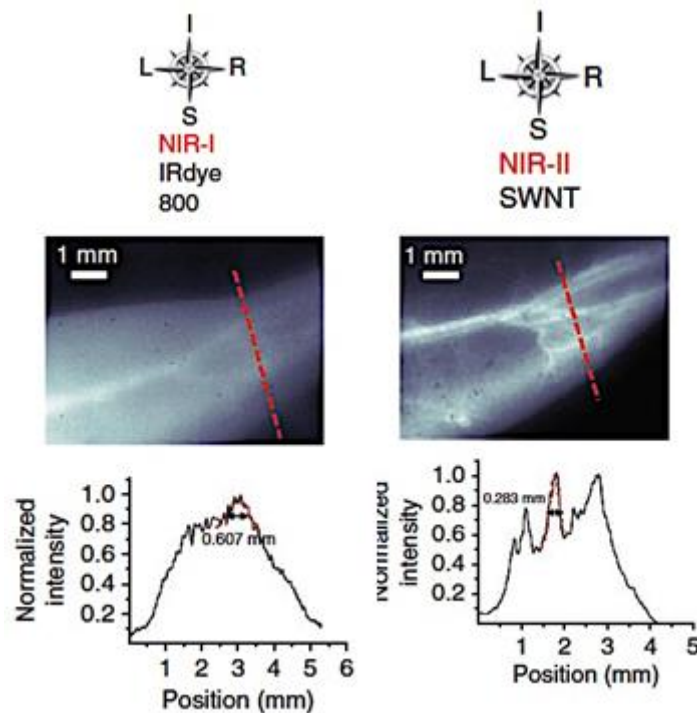


Figure 5. NIR-I fluorescence image (top left) and cross-sectional fluorescence intensity profile (bottom left) along red-dashed line of a mouse injected with the SWNT-IRDye-800 conjugates. Gaussian fit to the profile is shown in red dashed curve. NIR-II fluorescence image (top right) and cross-sectional fluorescence intensity profile (bottom right) along red-dashed line of a mouse injected with the SWNT-IRDye-800 conjugates. Gaussian fit to the profile is shown in red dashed curve, ¹⁰.

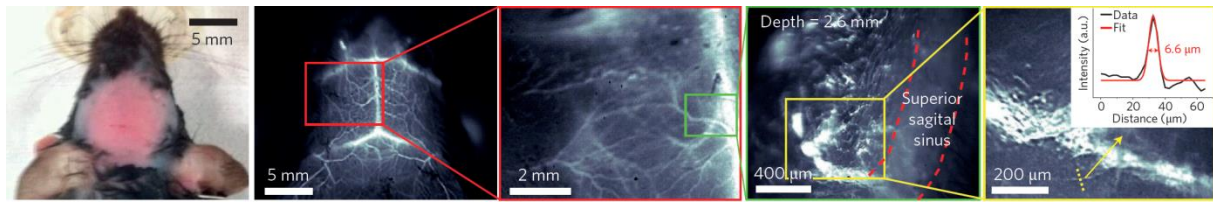


Figure 6. A C57Bl/6 mouse head with hair removed Low-magnification cerebral vascular image taken with a field of view of 25 mm× 20 mm. Cerebral vascular image of the same mouse head zoomed into the left cerebral hemisphere, with a field of view of 8mm×6.4mm. Cerebral vascular image of the same mouse head taken using a microscope objective, with a field of view of 1.7 mm× 1.4 mm. The depth of these in-focus vascular features was determined to be 2.6 mm. Zoomed-in image of a sub-region in f taken by a higher-magnification objective, with a field of view of 0.80 mm× 0.64 mm. Inset: cross-sectional intensity profile (black) and Gaussian fit (red) along the yellow-dashed bar, ¹¹.

Moungi G. Bawendi's team working at MIT achieved high temporal resolution looking at brain micro vascularization thanks to one of the brightest SWIR contrast agent known as InAs core quantum dots. This enabled to perform 3D image reconstruction and blood flow mapping (Figure 7) ¹².

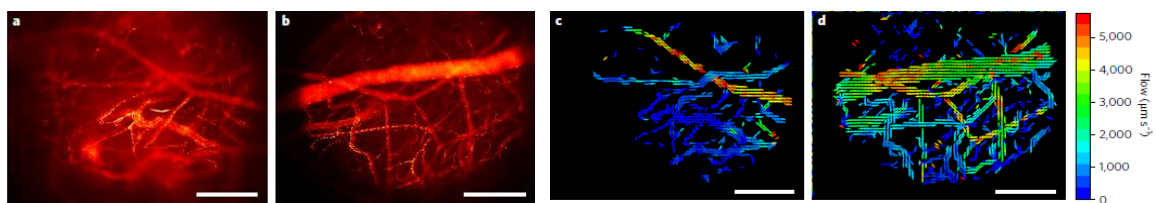


Figure 7. High-resolution, high-speed SWIR intravital imaging to generate flow maps of microvascular networks using QD composite particles. a–d, Applying a multi-pass particle image velocimetry approach to the images of the tumour margin (a) and healthy hemisphere (b) generated a flow map for each slice (c, d); coloured arrows indicate the direction and velocity of flow. Scale bars are 300 μm, ¹².

CTET/IAB in Grenoble develops research lines related to optical instruments for clinical translation. They already developed tools for the NIR-I called Fluobeam® (Figure 8) and FluoSTIC® which are today commercialized by the company Fluoptics and clinically used for real time guided surgery. Their applications have been described previously (see end of the framework section).

The Fluobeam®800 which was used for comparison with the SWIR platform is able to monitor fluorescent probes with a maximum absorption between 750nm and 800nm and a maximum emission between 780nm and 850nm. The excitation is provided by a class 1 expanded laser source at 780nm. The fluorescence signal is collected by a CCD through a high pass filter with a high transmittance for wavelength >830nm.



Figure 8. Fluobeam®.

During my internship I have been involved in a transdisciplinary project supported by the Plan Cancer oriented towards the development of SWIR imaging for biomedical applications. I was in

charge of the assembly and calibration of the SWIR imaging platform (Figure 9), which is the first milestone of this project. My aim was to optimize the excitation source and camera's parameters (hardware and software) by testing different contrast agents in capillaries within phantoms (agarose solutions mimicking optical tissue properties), and then testing them *in vivo* in mice. In parallel one of my tutors Xavier Le Guével provided new SWIR biocompatible contrast agents to be tested on this SWIR platform. The next step of the project, not scheduled in my master, will focus on the investigation of lymphatic and blood networks on wild type and pathological mice models. It will start by the study of the physiology of these networks, then the study of angiogenesis in cellulose sponge models and eventually lymphatic flow and drainage. The final milestone deals with image treatment and analysis using algorithms to achieve high spatial resolution, flow mapping and 3D reconstruction.

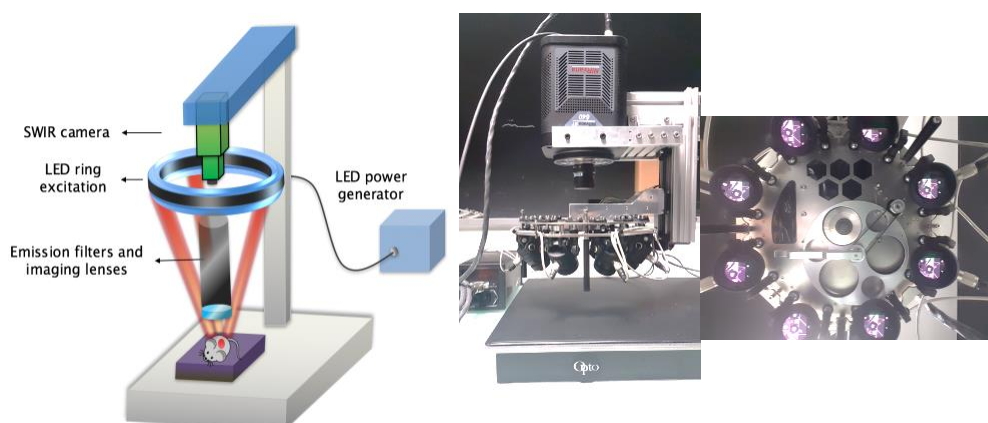


Figure 9. SWIR platform and LEDs excitation ring.

1- Assembly of optical bench and SWIR camera

1.1. Light source

The light source is a LED excitation ring surrounding the camera's field of view (Figure 10) rather than laser excitation because the room dedicated to the SWIR platform did not meet laser safety requirements and previous experiments in collaboration with CEA enabled to develop of an LED based large homogeneous illumination.

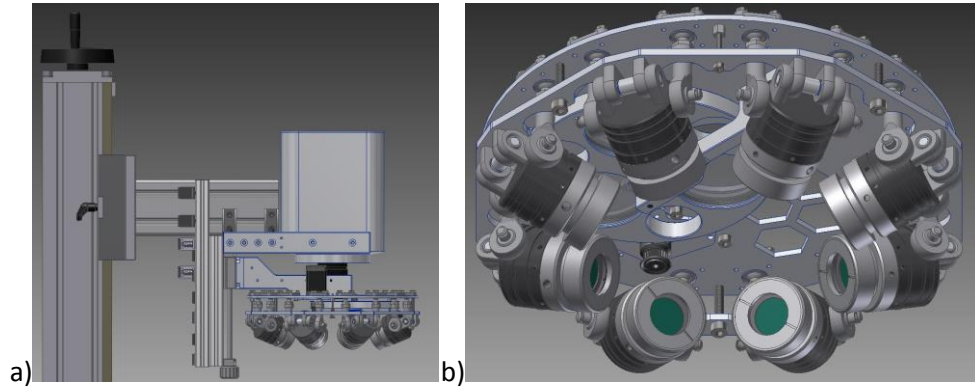


Figure 10. Industrial design of a) the SWIR platform and b) the excitation ring.

The light ring contains 8 High-Power LEDs. There are two groups of LEDs with two different wavelengths: LXML-PF 01, 720 nm, 260 mW and SFH4780S, 810 nm, 2900 mW/sr. Their spectral resolutions are illustrated below (Figure 11). These two wavelengths enable to excite different types of fluorophores described in subsection 2.1 by getting closer to their maximum absorption bands.

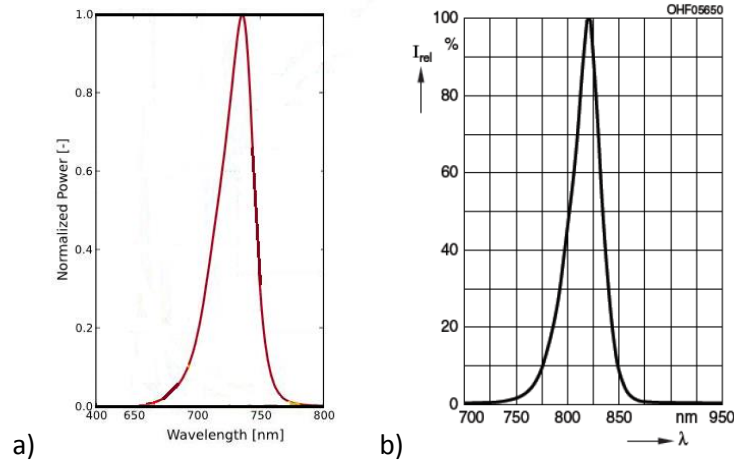


Figure 11. a) 720 nm and b) 810 nm LEDs spectra.

The LEDs can be dimmed with a Controller via an Rs232- Connection. The Controller is a Gardasoft RT-260 – Controller (Figure 12). For all the experiments, the LEDs have been used in continuous mode (Appendix: SWIR platform operation manual). LED are controlled in current and limited to 1A.

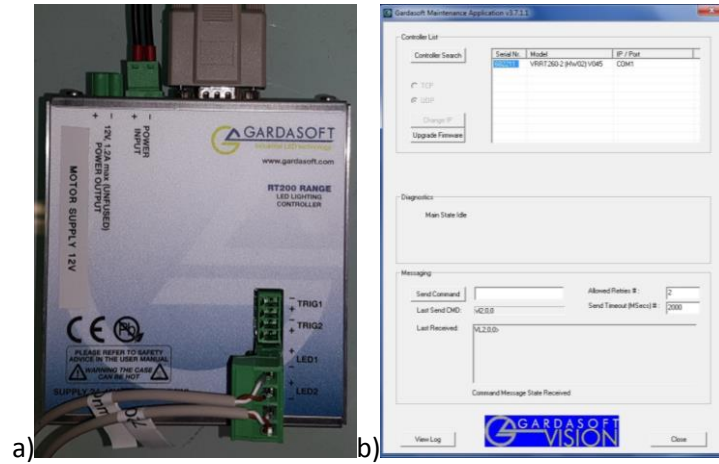


Figure 12. a) Gardasoft RT-260-Controller and b) its interface.

Concerning the excitation power, other research groups used incident powers between 50 and 160 mW/cm^2 ^{11,13–15,17}. However, to reach those values they used a 10 Watt LASER as excitation source. The excitation beams used for the CTET SWIR platform can be oriented by tilting the LEDs towards the center using three screws placed at 120° of each other around the light ring (Figure 13). When superimposed at 1A and 100% of brightness the LEDs reach 8.5 mW/cm^2 for the λ_{exc} 720 nm and 27 mW/cm^2 for the λ_{exc} 810 nm at a distance of 15 cm from the work plan (Figure 14). The lack of power has been a limitation during our experiments and to collect enough photons on the camera especially due to the low brightness of existing SWIR probes. Nevertheless the LEDs provided a homogeneous excitation area of 70 mm diameter (Figure 14), approximately the size of a whole mouse used for *in vivo* studies.



Figure 13. Tilting system of the LEDs.

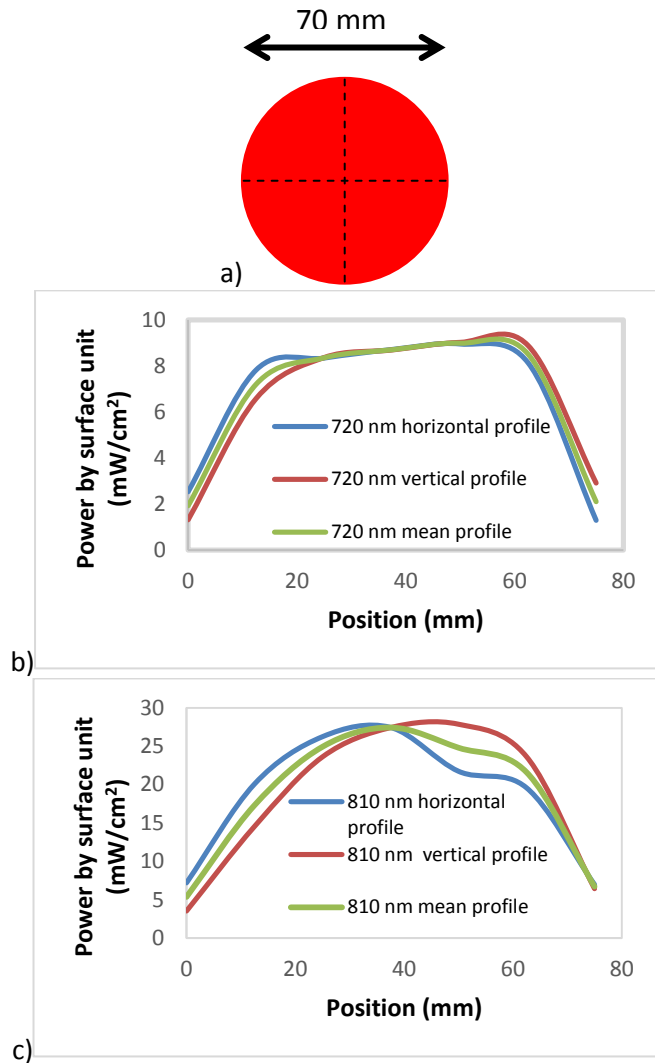


Figure 14. a) Illumination patch on the work plan. b),c) Intensity profiles along diameters of the circular excitation patch on the work plan. The left graph is for λ_{exc} 720 nm. The right one is for λ_{exc} 810 nm.

The light ring contains low risk LEDs. According to the IEC-62471-1 standard they belong to the group 1 in terms of risks. The hazard values are reported at a fixed distance $d = 200$ mm. There is no need to wear infrared protective glasses. The only safety caution is to not stare into the light.

1.2. Optics

The optical bench includes the different optical components (filters, lenses...) between the excitation source (1.1) and the SWIR camera. At the exit of each LED is placed a 1000 nm short pass filter from Thorlabs. This excitation filter is used to prevent wavelengths longer than 1000 nm to reach the sample (Figure 15, Figure 16). Under illumination, the fluorescent object starts emitting photons in addition to the reflected ones. Both are collected in front of the camera by a long pass filter called emission filter (Figure 15). This way, when the cut off wavelength of the emission filter is higher than the excitation filter's one, the excitation light is blocked by the emission filter and the camera only collects photons emitted from the fluorescent object.

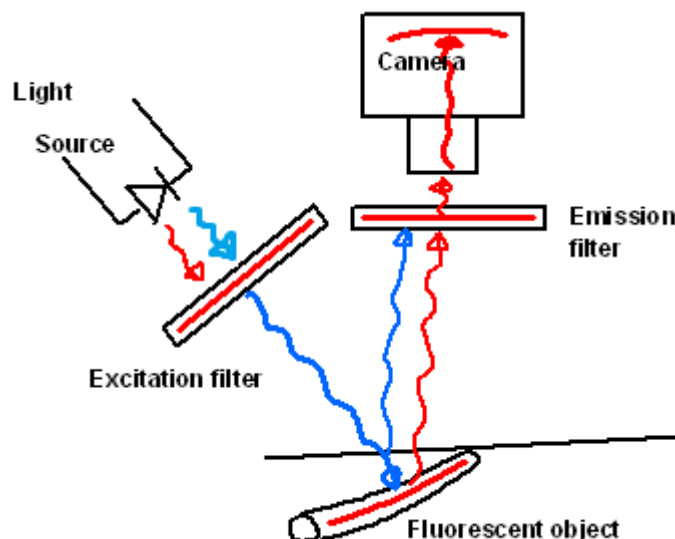


Figure 15. Principle of the optical bench.

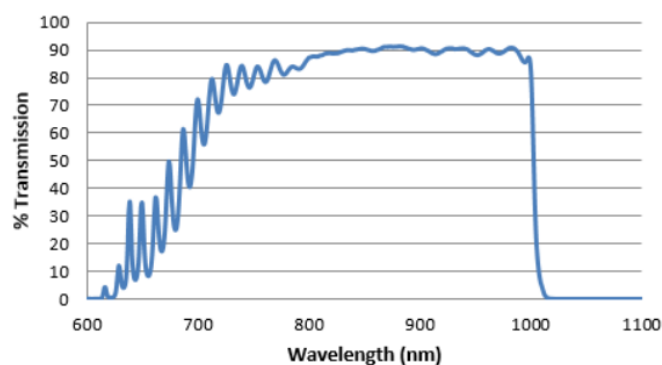


Figure 16. 1000 nm short pass transmission.

The platform is equipped with three types of long pass filters: 850 nm, 1000 nm and 1300 nm placed on a wheel in front of the camera. The LP 850 nm is the less selective filter. It is used for fluorophores exhibiting weak signal above 1000 nm. Indeed only few SWIR contrast agents are available and some NIR-I fluorophores may be used as SWIR probes thanks to the tail of their emission spectrum^{8,17}. However, we reckon this filter not being suitable for optimizing the SWIR platform because it is close to the NIR-I window traduced by high scattering and tissue autofluorescence. The LP 1000 nm is a good compromise between the two others. It is the first filter which enables to work in the SWIR. The LP 1300 nm filter was bought to go further in the NIR-II to demonstrate the reduced autofluorescence and scattering in this region. These two last filters have been chosen with an optical density above 4 ($OD > 4$), which means a percentage of transmission lower than 0.01% in the blocking window for high performance of the filter (Figure 17).

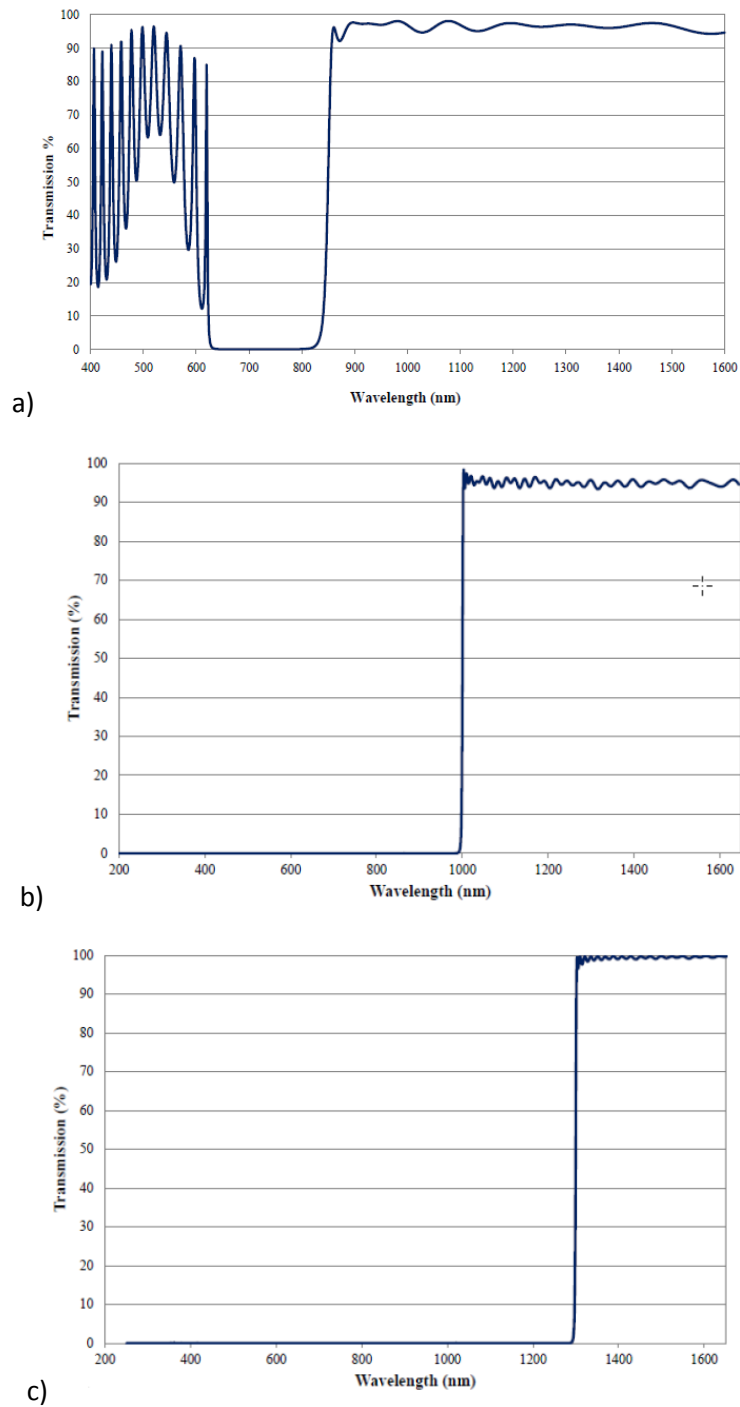


Figure 17. Transmission spectra of the a) LP 850 nm, b) LP 1000 nm and c) LP 1300 nm. LP 850 nm has a coating performance $OD > 2.0$ whereas LP 1000 nm and 1300 nm have $ODs > 4.0$ which is for high blocking performances.

The emitted photons are collected by the camera through Navitar SWIR lenses (Figure 18) providing a transmission higher than 75% in the 900-1700 nm window. Three sets of lenses with focal distances of 12.5 mm, 25 mm and 50 mm enable to work at different distances and magnifications. In order to obtain the highest light power in our samples, we chose to place the system light ring/camera as close as possible from the work plan. A distance of 15 cm between the plan and the bottom of the LEDs seems to be reasonable to allow hand manipulation of mice under the camera. The 25 mm lens turned out to be the most appropriate to image a full mouse at this distance. To

maximize the intensity of the recorded signal, all pictures are taken with the diaphragm of the lens completely opened at 1.4 and varying the exposure times.



Figure 18. Navitar SWIR lens.

1.3. Camera

The camera selected for the SWIR platform is the NIRvana: 640ST from Princeton Instruments imaging group (Figure 19). The chip is 640x512 Indium Gallium Arsenide (InGaAs) array, which offers a high resolution in the SWIR region. The quantum efficiency response is practically a plateau around 85% from 900 nm to 1700 nm (Figure 20). Its 20 μm x 20 μm pixels offers a high spatial resolution. During operation the detector is cooled thermoelectrically at -60°C by a Peltier device. At this temperature, the dark current created is around 1500 $\text{e}^-/\text{p}/\text{sec}$. The digitization is performed on 16 bits by the A/D converter. Three scan rates are available: 2 MHz, 5 MHz and 10 MHz. An electronic shutter enables to precisely control the integration times.



Figure 19. Princeton Instruments: NIRvana 640ST.

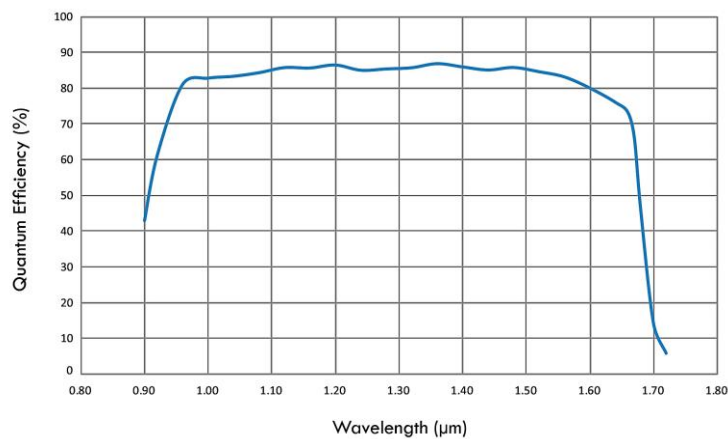


Figure 20. Quantum efficiency of the NIRvana 640ST's InGaAs chip versus wavelength.

The image and video acquisition are performed by Lightfield software. It enables to set the picture parameters such as the exposure time per frame, the number of exposure per frame in case the picture has to be averaged, the saving location and format. The camera settings such as the amplification gain, scan rate are also controlled through the interface (Figure 21). Because of the weak emission of the SWIR probes, the gain of the detector is set to high to amplify the signal as much as possible. However, the A/D converter cannot work at high gain and high scan rates at the same time because of its technical limitations. Since most of the experiments of the internship do not require high temporal resolution the scan rate is set to 2 MHz, its lowest value.

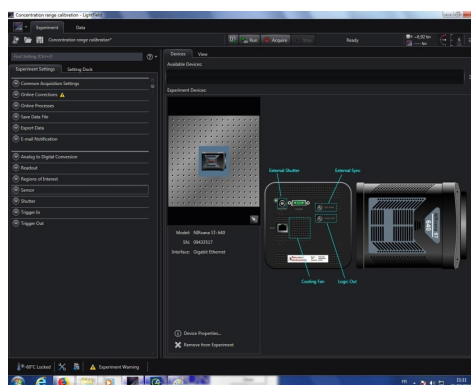


Figure 21. Lightfield interface.

To reduce the background, an average image of a hundred exposures is taken in the dark without sample and light ring illumination in the same conditions than the following experiment (same exposure time, emission filter, lens settings). Then when the picture of the sample under LEDs' illumination is taken, the image of the background previously acquired is subtracted. A clean image without background noise is obtained. An averaged preliminary image has to be taken in the same conditions except the excitation light ring has to be turned ON at the same wavelength, intensity and brightness that will be used for the experiment.

The images taken on the SWIR platform are compared to the ones from the Fluobeam® 800 (Figure 8). We summarize the specifications of both systems in Table 1.

	Fluobeam® 800	NIRvana 640ST
Integration	Fixed ceiling laser class M Irradiance on the imaging field: 8.5 mW/cm ² @ 16 cm	Movable light ring, LED Risk Group 1 (Low Risk) according to IEC-62471-1 720 nm: 8.5 mW/cm ² @ 15 cm 810 nm: 27 mW/cm ² @ 15 cm
Detector chip	Si CCD (780-850 nm → NIR-I)	InGaAs CCD (900-1700 nm → SWIR)
Thermoelectric cooling	No	Yes (-60°C)
Field of view	7.5cm x 10 cm	Object Area (mm) at 192 x M.O.D. (HxV) 1" 144 Object Area (mm) at 96 x M.O.D. (HxV) 1/2" 72 Object Area (mm) at 132 x M.O.D. (HxV) 2/3" 99
Pixels Number	316 000	327 680
Working distance	20cm	30 cm
Resolution	4 Cycles /mm	20 µm x 20 µm pixels
Scan rate	NA	2 MHz
Pixel well capacity (e⁻)	NA	High Gain ≥ 40 000
Dark current (e⁻/p/sec)	NA	~1500 @ -60°C
Visible image	No	No
Zoom	No	Yes (manual)

Table 1. Comparison between Fluobeam® 800 and NIRvana 640 ST.

2- Testing SWIR contrast agents and comparison with NIR imaging systems

2.1. SWIR probes

We select different fluorophores emitting in the SWIR region either developed by us and collaborators or commercially available. These SWIR probes can be listed in two classes : 1) metallic particles, 2) organic dyes.

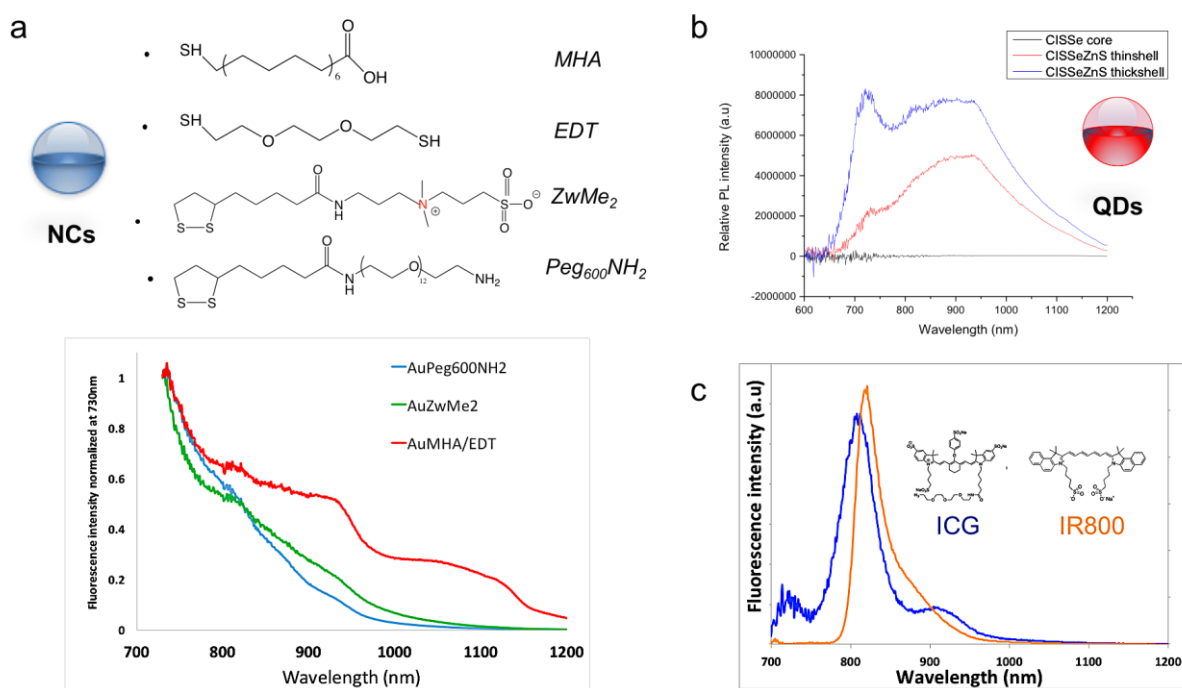


Figure 22. a) Series of Au NCs : AuPeg600NH₂, AuZwMe₂, AuMHA/EDT and their fluorescence emission profiles (1 mg Au/mL in water, λ_{exc} 450nm). b) Fluorescence emission of QDs at each synthesis step (0.1 mg /mL in hexane, λ_{exc} 450nm). c) ICG and IR800 formula and fluorescence emission spectra (0.1 mg /mL in PBS, λ_{exc} 700nm).

2.1.1. Metallic particles

Researchers at CTET works actively on new emitters in the NIR-I/SWIR window made of ultra-small gold particles (size <3nm) called also gold nanoclusters (Au NCs). These species have metal core core stabilized by small molecules such as thiol organic molecules or biomolecules (peptides, oligonucleotides). The synthesis is quite straightforward and gives high yield of water-soluble particles. Their photoluminescence is highly dependent of the metal core size and the nature of the ligands (i.e stabilizing molecules). It was shown recently that Au NCs stabilized by zwitterionic molecules exhibit an intense emission centered at 1000nm¹⁶. In this context, we use in this project 3 types of Au NCs stabilized by different ligands. The best candidate called Au-MHA/EDT is composed of gold core stabilized by 2 distinct thiol ligands (MHA : mercaptohexanoic acid ; EDT : ethylenedithiol) enabling a relatively high photoluminescence in the SWIR region above 1300 nm. The two other types of Au NCs are prepared using a thiol pegylated chain with a terminal amine groups AuPeg₆₀₀NH₂ and a bidentate zwitterionic molecules AuZwMe₂. Cartoon of the ligands and emission spectra of these Au NCs are illustrated in Figure 22a.

As a second type of inorganic particles, we test the Quantum Dot CISSeZnS made of Indium (I), copper (C), Zinc (Zn) and Selenium (Se) from our collaborators at CEA/INAC (Davina Moodely/Peter Reiss). This Quantum Dot exhibits very strong and broad emission centered at 900nm with a

photoluminescence signal detected to the wavelengths >1300nm (not shown here). Emission profile of CISSeZnS (1mg/mL in hexane; $\lambda_{\text{exc.}}$ 450nm) is depicted in Figure 22b.

2.1.2. Organic dyes

There is a high interest to move from inorganic to biodegradable and biocompatible SWIR probes. Very recently, a study¹⁵ demonstrated the ability to detect FDA approved organic dyes Indocyanine Green (ICG) and IR800Cw in the SWIR region. We then purchase these compounds and test them in our set of experiments. Figure 22c shows the molecules and the emission profiles of ICG and IR800 dye. It should be noted that, despite a quite similar emission profile with almost no photoluminescence signal above 1200nm, IR800 is 10 times brighter than ICG at the same concentration (0.01 mg/mL in PBS) in the SWIR window.

2.2. SWIR probes in intralipid phantom

The first series of experiments were performed using intralipid phantoms made of agarose and intralipid. These phantoms mimic the biological tissues absorption and scattering properties and we aim to detect signal of contrast agents inserted at different depths in these phantoms using the SWIR platform and the Fluobeam® 800.

The phantom solution is prepared by dissolving 150 mg of agarose in a 15 mL aqueous solution 1% intralipid on a hot plate stirring during 15 minutes. Once the agarose is dissolved the solution is poured in a cylindrical mold where a guiding capillary is tensed at the desired height. Then the mold is left in ice for few minutes to speed up the cooling and jellification (Figure 23). Eventually the guiding capillary is removed leaving a straight tunnel at a fixed depth in the phantom where a new capillary filled with contrast agent will be inserted to acquire images (Figure 24).



Figure 23. Protocol of phantom synthesis from left to right: solution preparation, agarose dissolution on hot plate and molding.

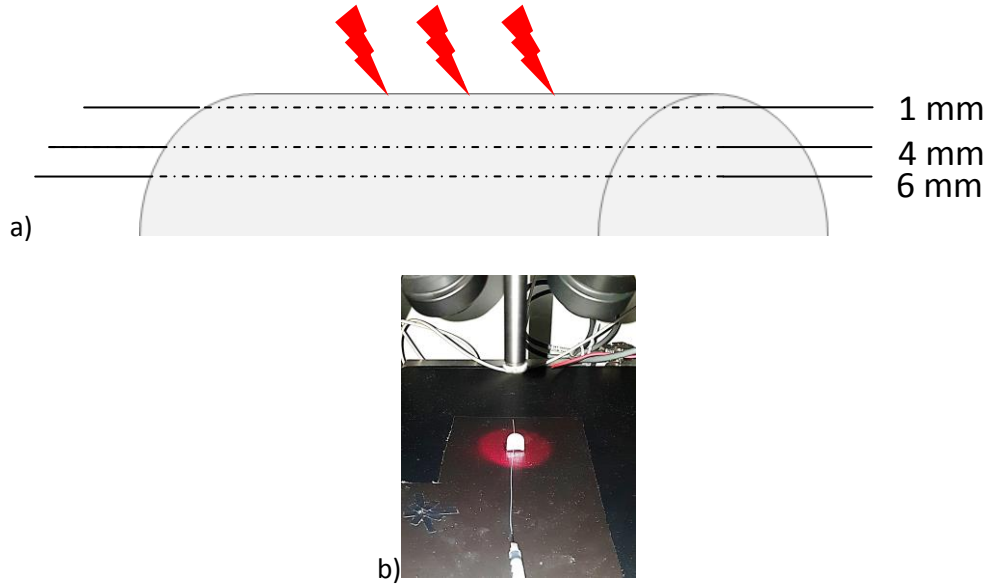


Figure 24. a) Intralipid phantom schematic under LED excitation showing the different depths at which the SWIR probes were tested. b) Picture of the experiment.

Series of pictures are taken at different exposure times: 1ms, 5ms, 10ms, 25ms, 50ms, 100ms, 200ms, 500ms, 1000ms. Both excitations (720 nm, 810 nm) are successively combined with LP 1000 nm and LP 1300 nm emission filters. The samples were also imaged with the Fluobeam® 800 at the same exposure times. These acquisitions are repeated for capillaries containing the contrast agents placed outside the phantom and at 1 mm, 4 mm and 6 mm in the phantom (Figure 24).

Before testing any contrast agent the first bench of experiments aimed to study the 1% intralipid phantom autofluorescence. In this case the capillary was filled with PBS. On Figure 25 are plot the ratios between phantom's autofluorescence and the surrounding background. The goal of this ratio is to be the closest as possible to the limit of detection which is 1. In the ideal case the autofluorescence of the phantom would not be detectable because at the same level as the background noise. The LP 1300 nm shows a lower autofluorescence of the phantom compared to the LP 1000 nm (Figure 25). Nevertheless, this filtering seems to be more efficient for λ_{exc} 720 nm than for λ_{exc} 810 nm (Figure 25). This is certainly due to the fact that the excitation short pass filter has not a cut off performant enough to suppress wavelengths above 1000 nm in the λ_{exc} 810 nm spectrum.

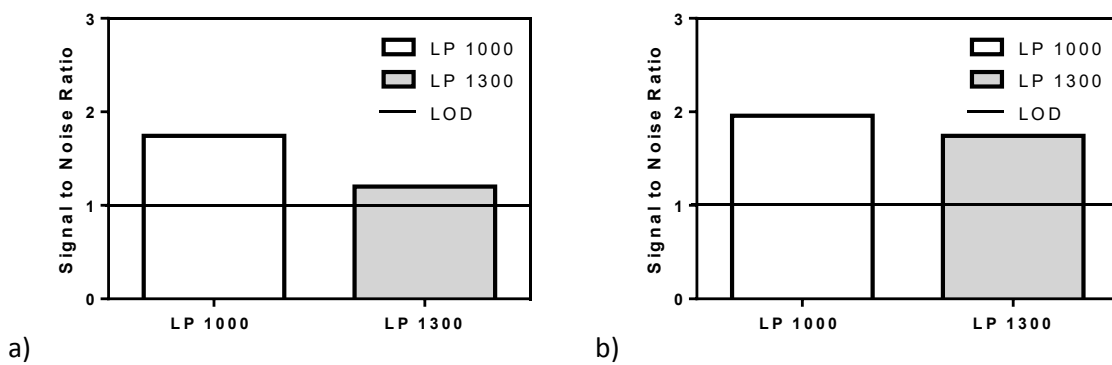


Figure 25. 1% intralipid phantom autofluorescence measured on SWIR platform with LP 1000 nm and 1300 nm filters, 200 ms exposure time: a) λ_{exc} 720 nm b) λ_{exc} 810 nm.

The first contrast agent studied in phantoms is the gold nanoclusters AuMHA/EDT at 1mg Au per mL and will be the reference compound for the following experiments. It was tested with Fluobeam®800 and NIRvana 640 ST under the conditions reported below (Figure 26). The values of fluorescence are normalized with respect to the one taken outside the phantom (0 mm). In all configurations, the signal is detected until 6 mm and was not tested deeper. We observed a decrease of the fluorescent signal at higher depth in the phantom due to the enhancement of absorption and scattering. The signal detected at 6 mm by the SWIR system at λ_{exc} 810 nm (27.87% for LP1000 and 17.27% for LP1300) was greater than those measured at the same depth with Fluobeam®800 (18.69%) and the SWIR system at λ_{exc} 720 nm (21.19% for LP1000 and 10.13% for LP1300) (Figure 26). Indeed the 810 nm was the most powerful available excitation wavelength. Therefore it is more likely to transmit a high intensity to the camera through the fluorescence process of the contrast agent. Reflections on the phantom also contribute to this phenomenon since the excitation is not completely filtered because of the low quality of the short pass filters. Concerning the histograms b) and c) the LP 1300 nm emission filter transmits a weaker signal to the camera compared to the LP 1000 nm. It enables less photon to pass through because of its more restricted spectral window.

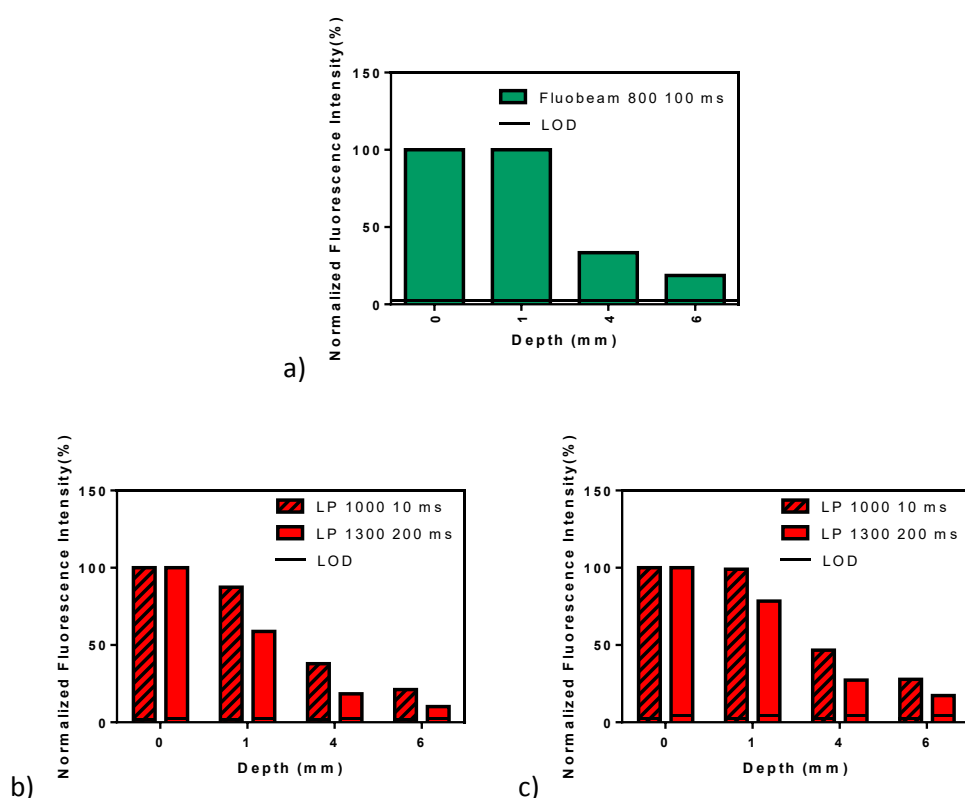


Figure 26. Normalized fluorescence intensity of AuMHA/EDT (1 mg Au/mL) versus depth in 1% intralipid phantom: a) Fluobeam®800, λ_{exc} 780 nm, 100 ms exposure time for LP 830 nm, b) SWIR platform, λ_{exc} 720 nm, 10 ms exposure time for LP 1000 nm, 200 ms exposure time for LP 1300 nm, c) SWIR platform, λ_{exc} 810 nm, 10 ms exposure time for LP 1000 nm, 200 ms exposure time for LP 1300 nm.

A similar behavior could be observed using organic compounds like ICG and IR 800 (Figure 34, Figure 35) excepted measurements could be performed only with LP 1000 nm due to the absence of detection with LP 1300 nm.

Another important aspect demonstrated on the following graph (Figure 27) is that a given depth to be imaged is linked to an optimum exposure time. One can notice that the exposure time corresponding to the highest signal to noise ratio in each group increases with depth. This comes from the fact that saturation is reached at longer times when signal is emitted from deeper since it is weaker.

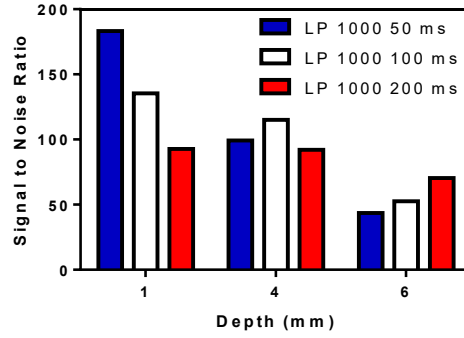


Figure 27. Signal to Noise Ratio of IR 800 versus depth on SWIR platform, λ_{exc} 720 nm, LP 1000 at 50, 100 and 200 ms exposure times.

2.3. SWIR probes under chicken slices

This experiment consisted in testing the in depth detection sensitivity of the system using chicken slices as biological tissue. We chose the same setting used for the phantom experiments with AuMHA/EDT as contrast agent (1mg Au/mL). Instead of testing capillaries in phantoms, 2 mm thick chicken slices bought from supermarket are successively stacked over the capillary (Figure 28). The series of pictures are taken at 0 mm, 2 mm, 4 mm, 6 mm and 8 mm.

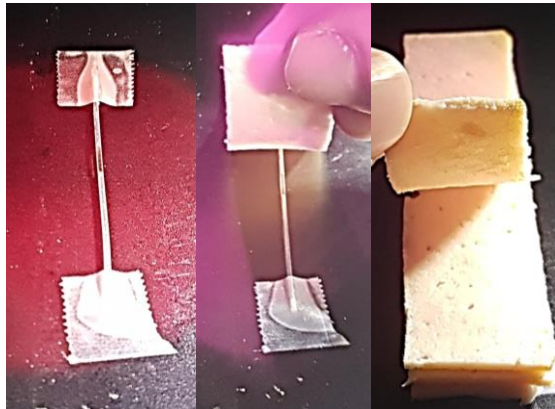


Figure 28. AuMHA/EDT (1mgAu/mL) capillary under excitation (left). Chicken slice staking over the capillary (middle and right).

The signal detected decreased faster with depth using chicken than in phantom (Figure 29) with no specific signal detected above 4 mm depth in tissue. As for the previous experiment, the signal measured with the SWIR system at λ_{exc} 810 nm decreased slower than the one measured at λ_{exc} 720 nm while increasing the depth. This can still be explained by the higher power of the λ_{exc} 810 nm.

However, due to low quality of the short pass 1000 nm this high power contributes to raise the noise level since excitation is not well filtered and reaches the camera. Thus detection is not improved with λ_{exc} 810 nm compared to λ_{exc} 720 nm even if it should be. Moreover it seemed that LP 1000 nm provided a better signal to noise ratio than LP 1300 nm until 2 mm especially for λ_{exc} 720 nm.

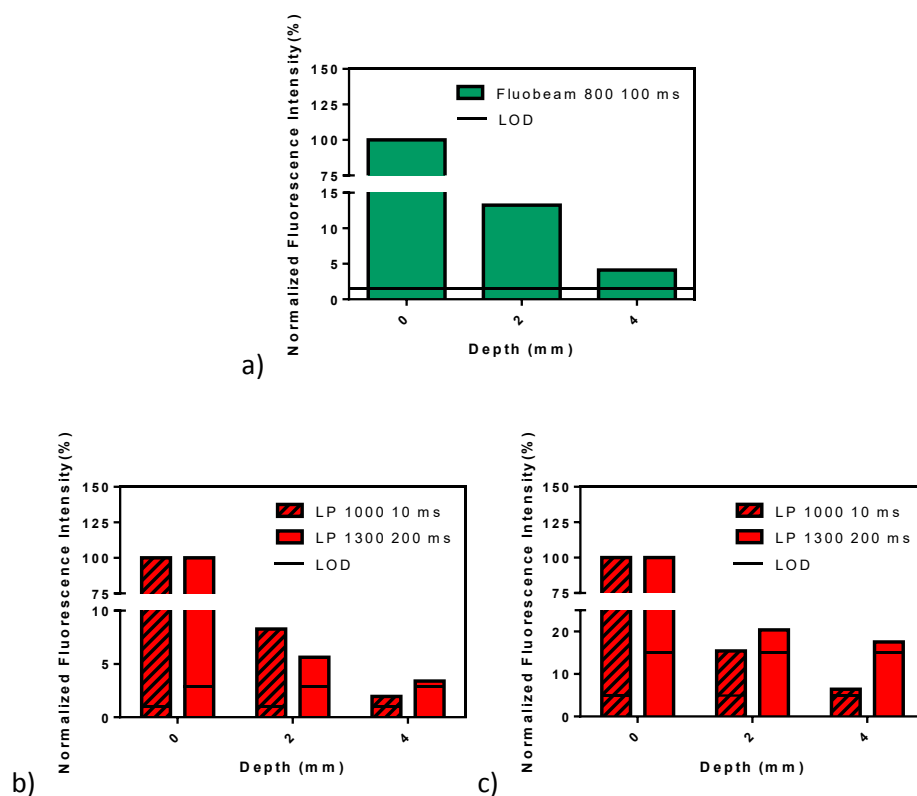


Figure 29. Normalized fluorescence intensity of AuMHA/EDT (1 mg Au/mL) versus depth under chicken slices: a) Fluobeam®800, λ_{exc} 780 nm, 100 ms exposure time for LP 830 nm, b) SWIR platform, λ_{exc} 720 nm, 10 ms exposure time for LP 1000 nm, 200 ms exposure time for LP 1300 nm, c) SWIR platform, λ_{exc} 810 nm, 10 ms exposure time for LP 1000 nm, 200 ms exposure time for LP 1300 nm.

2.4. In vivo studies with capillaries

The *in vivo* studies performed in the last part of the internship aimed to evaluate the sensitivity of detection of SWIR photoluminescence in mice. The wavelength chosen for this part was λ_{exc} 810 nm since it is the most powerful available on the SWIR platform and moreover it is the longest thus it is supposed to penetrate deeper in the tissues.

As expected, autofluorescence of mice skin showed an obvious decrease closer to the LOD using the LP at longer wavelength as seen in Figure 30. Consequently, the selection of LP1300 seems more suitable to reduce the background level.

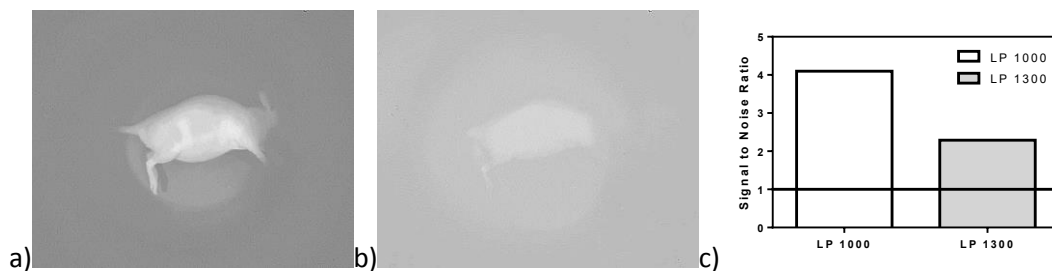


Figure 30. Nude mouse skin autofluorescence measured on SWIR platform with a) LP 1000 nm and b) 1300 nm filters, 200 ms exposure time, λ_{exc} 810 nm. c) Signal to noise ratio of autofluorescence on background.

Capillaries were filled with 3 gold nanoclusters ($AuPEG_{1000}NH_2$, $AuZwMe_2$ and $AuMHA/EDT$ at 2.5 mg Au/mL) and ICG (0.1 mg/mL) and inserted under the mice skin. A small incision was made in the flank of the mouse under isoflurane anesthesia and the skin was carefully detached from the underlying muscular tissues. Then the capillaries were successively inserted and imaged (Figure 31). Plotting the signal to noise ratio, which is the ratio between the SWIR probe fluorescence and the mouse skin autofluorescence, revealed that the $AuMHA/EDT$ was three times brighter than the two other gold nanoclusters both with the LP1000 and the LP1300, thirty times brighter than ICG under LP1000 and six times brighter than ICG using LP1300 (Figure 31).

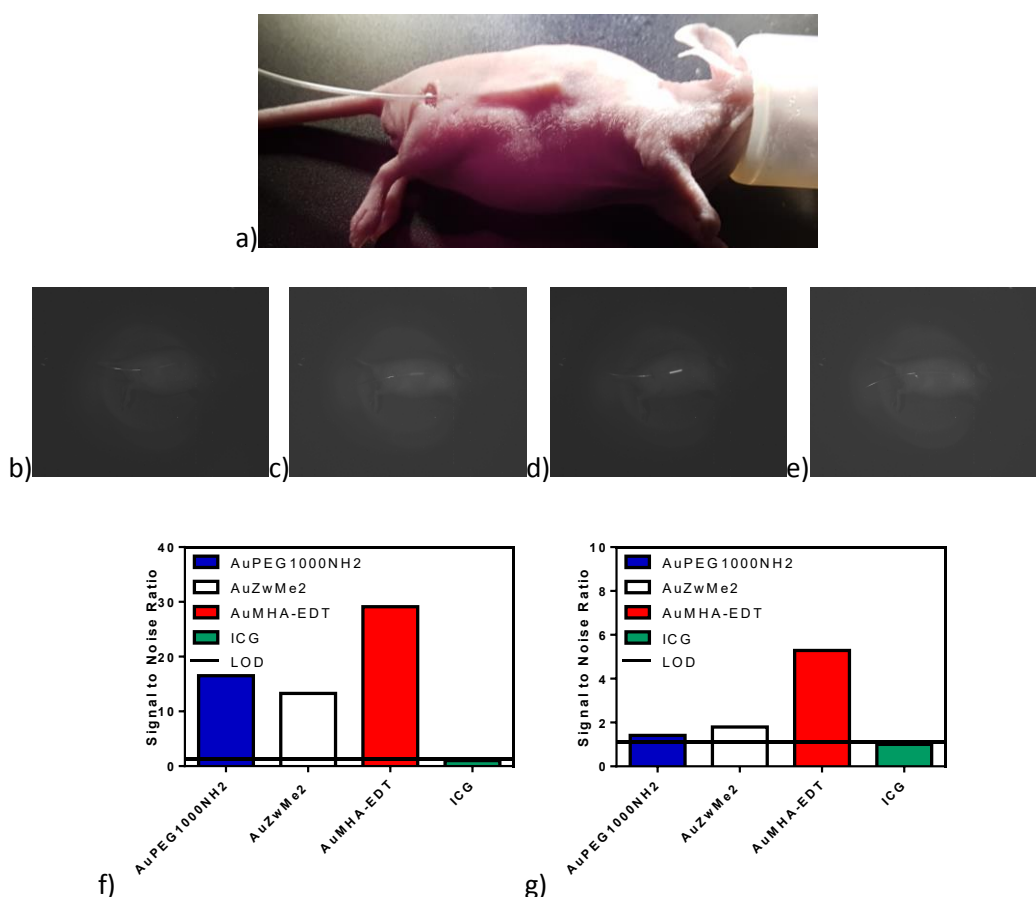


Figure 31. a) Subcutaneous capillary experiment. b)-e) $AuPEG_{1000}NH_2$, $AuZwMe_2$, $AuMHA/EDT$ 1.5/0.5, 2.5 mg Au/mL and ICG 0.1 mg/mL subcutaneous capillaries in mice, LP 1300 nm, 200 ms exposure time, λ_{exc} 810 nm. Signal to Noise Ratio of the previously described (b-e) contrast agents f) under LP 1000 nm, g) under LP 1300 nm.

The next step was to insert the capillaries deeper in the body to determine the limit depth of detection *in vivo*. The contrast agent used for this experiment was a quantum dot (QD) made in

collaboration with CEA since it is brighter than the AuMHA/EDT nanocluster even if it was soluble only in cyclohexane.

Intra rectal insertion of the capillary revealed some diffuse signal from the QD at 10 ms exposure time with LP 1000 nm whereas nothing was detected from AuMHA/EDT under same excitation conditions at any exposure time (Figure 32).

Intra tracheal insertion did not enable the detection of any contrast agent used during the internship. Thus the best depth reached by this *in vivo* study is within the abdomen at approximately 7 mm in depth when ventral side of the mouse is exposed.

Despite a relatively good sensitivity of detection for AuMHA/EDT and the QDs using LP1300, we can consider that there is a high need of brighter biocompatible SWIR probes for *in vivo* detection.

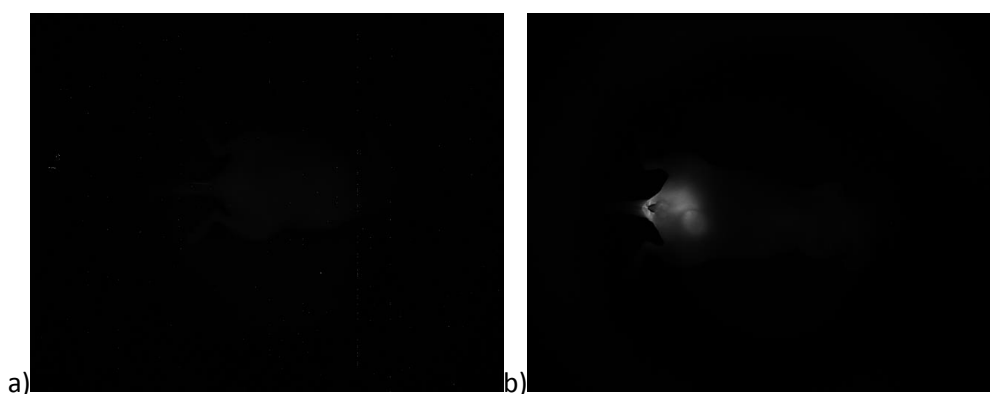


Figure 32. a) AuMHA-EDT 2,5 mg Au/mL, ventral side intra-rectal, λ_{exc} 810 nm, LP1000nm 10 ms. b) QDs, ventral side intra-rectal, λ_{exc} 810 nm, LP1000nm; 10 ms.

2.5. Models' comparison

This part aims to compare the previously developed models (phantoms, chicken slices and subcutaneous insertion) in terms of spatial resolution to check the hypothesis that filtering the emission at longer wavelength should reduce the scattering and thus improve the spatial resolution. The intensity profile of the relative fluorescence is plot along a section cutting the capillary perpendicularly in each model. The contrast agent used was AuMHA/EDT under λ_{exc} 810 nm, 10 ms exposure time for LP 1000 nm and 200 ms for LP 1300 nm since this settings have comparable fluorescence intensity. When normalizing the fluorescence intensities between the LP filters, one can notice that there was no real difference between the LP 1000 and LP 1300 in the case of phantom (Figure 33a)). However profile b) demonstrated a slight improvement of the LP 1300 nm pic sharpness with respect to the LP 1000 nm while the difference was clear for profile c) (Figure 33). Consequently profiles b) and c) support the hypothesis that spatial resolution is improved when shifting the window towards higher wavelengths in SWIR. Moreover it also illustrated that the phantom model used to mimic biological tissues is not optimized yet.

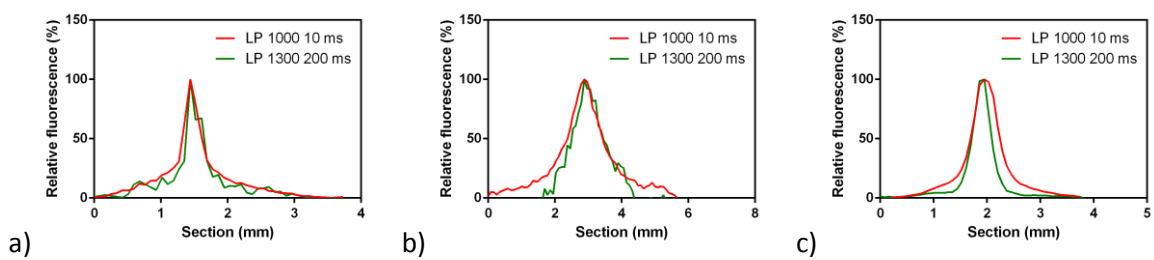


Figure 33. Relative fluorescence along a perpendicular cross section of a capillary filled with AuMHA/EDT 0.5/1.5 λ_{exc} 810 nm a) in 1% intralipid phantom 6mm deep, b) under chicken 2 mm deep, c) as subcutaneous implant in mouse depth < 1mm.

3- Discussion

During this internship, the first milestone has been to assemble and calibrate the SWIR platform. Here is the part of my internship where I had to face engineering problems with the subcontractor who designed the optical bench and the excitation light ring. At the first delivery, the excitation LEDs did not have the right wavelengths (730/860 nm instead of 720/810 nm). The adapting C-mount rings to shorten the focal distances of the lenses were missing. The emission filters LP 1000 nm and LP 1300 nm were in reality cut band filters instead of long pass filters. Consequently the excitation light was not filtered well. Once these problems solved, I have been able to calibrate the LEDs to obtain a 70 mm homogeneous excitation disk on the work plan, the light ring being placed 15 cm above to enable *in vivo* manipulations.

In the following step, several contrast agents have been studied and it highlights that even if the detector technology is well developed, there is still a lack of good emitters in the SWIR window. The QDs made of Indium/copper is the brightest family of SWIR probes used in this study. However they face biocompatibility issue since they are stable only in hexane, which is toxic for the organism. FDA organic compounds such as ICG or IR 800 initially developed for the NIR-I demonstrated that they can be used in the SWIR windows thanks to the tail of their emission spectrum. Nevertheless they are not optimal for this window in terms of maximum excitation and emission. Another type of SWIR probes, gold nanoclusters made of approximately 25 to 100 atoms corresponding roughly to 3 nm in diameter are biocompatible and could be cleared by the kidneys. One of them, AuMHA/EDT showed interesting optical properties in the SWIR window that enable to optimize the SWIR platform during this project.

Testing AuMHA/EDT, ICG and IR 800 in 1% Intralipid phantoms demonstrated that the detection of signal became quickly critical when depth exceeded half centimeter. LP 1300 nm filters more photons than LP 1000 nm thus decreases not only the background and autofluorescence but also the signal of the probe. This is why probes' maxima of emission must be shifted towards higher wavelength to enable the LP to filter more the noise than the emitted signal from the probe. In parallel λ_{exc} 810 nm being more power full than λ_{exc} 720 nm, the fluorescence intensity detected under the first excitation is higher than the second one at a given depth. Therefore making the excitation light penetrate deeper in tissue requires high power. However the experiment on chicken slices stressed that powerful excitation was detrimental without the appropriate filtering of the emission because otherwise the LOD (background + autofluorescence) rises with the signal of interest and thus the SNR does not improve. Eventually, imaging deeper probes requires longer exposure time to reach optimal SNR.

The *in vivo* study and especially the intra rectal experiment revealed that it is difficult to collect a high resolute signal coming from more than half a centimeter in the body probably due to the heterogeneity of the organs that lead to strong photon losses. Nevertheless it was possible to reach high spatial resolution under skin. In this direction, there is a clear benefit to obtain a significant improvement of spatial resolution collecting photoluminescence emission at wavelength longer than 1300 nm instead of 1000 nm.

4- Protocol for new users of the SWIR platform

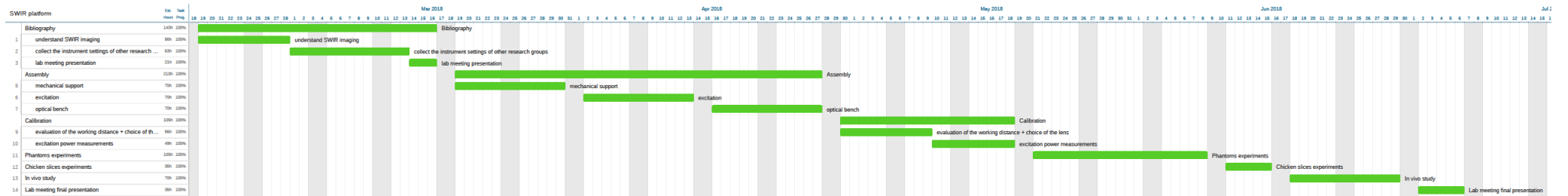
During the last part of my internship I also wrote an operation manual for the SWIR platform which is detailed in Appendix.

Conclusion

This internship enabled the assembly and first calibration of the SWIR imaging platform. Optimization of the platform showed the crucial role of a homogeneous and powerful excitation ($>20 \text{ mW/cm}^2$) in order to collect enough photon from the SWIR window and detect signal in vivo. Series of experiments using intralipid phantoms, chicken tissue and mice confirmed the benefit to detect signal at longer wavelengths ($>1300\text{nm}$) allowing a better spatial resolution due to the reduction of scattering and autofluorescence. Due to the high sensitivity of the SWIR camera, it appears also extremely important to improve the filtration of the excitation and the emission to enhance the signal to noise ratio and therefore the sensitivity.

Several upgrades of the platform are thus planned. In priority, the filtering will be improved. The 1000 nm short pass filters in front of the 720 nm and 810 nm LEDs will be replaced respectively with 750 nm and 850 nm high performance ($\text{OD}>4$) short pass filters. The emission filters will be directly mounted on the Navitar lens to filter all the light entering the camera and a color filter will be added on the emission filter wheel. Concerning the interface, the Lightfield software will be modified a little to ease the modification of image acquisition parameters and will be coupled to the Gardasoft excitation interface for more ergonomics. The purchase of a spectrometer that could be coupled to the NIRvana 640ST is also planned to study the probes spectrum in the SWIR window. To finish, new biocompatible and brighter SWIR probes are required to push this technology towards clinical translation.

Gantt Chart



Budget

SWIR Platform	100,000€ HT
Contrast agents	1,000€
Phantom,tissue	100€
Mice+experiment (technicien, anesthésia...)	800€
Shipping	500€
Trainee	2,625€
TOTAL	105,025€

Bibliography

1. Hirsjärvi, S. *et al.* Influence of size, surface coating and fine chemical composition on the in vitro reactivity and in vivo biodistribution of lipid nanocapsules versus lipid nanoemulsions in cancer models. *Nanomedicine Nanotechnol. Biol. Med.* **9**, 375–387 (2013).
2. Dufort, S. *et al.* Nebulized Gadolinium-Based Nanoparticles: A Theranostic Approach for Lung Tumor Imaging and Radiosensitization. *Small* **11**, 215–221 (2014).
3. Hitier, M., Cracowski, J.-L., Hamou, C., Righini, C. & Bettega, G. Indocyanine green fluorescence angiography for free flap monitoring: A pilot study. *J. Craniomaxillofac. Surg.* **44**, 1833–1841 (2016).
4. Christensen, A. *et al.* Feasibility of Real-Time Near-Infrared Fluorescence Tracer Imaging in Sentinel Node Biopsy for Oral Cavity Cancer Patients. *Ann. Surg. Oncol.* **23**, 565–572 (2016).
5. Falco, J., Dip, F., Quadri, P., de la Fuente, M. & Rosenthal, R. Cutting Edge in Thyroid Surgery: Autofluorescence of Parathyroid Glands. *J. Am. Coll. Surg.* **223**, 374–380 (2016).
6. Hong, G., Antaris, A. L. & Dai, H. Near-infrared fluorophores for biomedical imaging. *Nat. Biomed. Eng.* **1**, 0010 (2017).
7. MULTISPECTRAL IMAGING/DEEP TISSUE IMAGING: Extended near-infrared: a new window on in vivo bioimaging - BioOptics World. Available at: <https://www.bioopticsworld.com/articles/print/volume-7/issue-1/features/multispectral-imaging-deep-tissue-imaging-extended-near-infrared-a-new-window-on-in-vivo-bioimaging.html>. (Accessed: 4th August 2018)
8. Thimsen Elijah, Sadtler Bryce & Berezin Mikhail Y. Shortwave-infrared (SWIR) emitters for biological imaging: a review of challenges and opportunities. *Nanophotonics* **6**, 1043 (2017).
9. Smith, A. M., Mancini, M. C. & Nie, S. Second window for in vivo imaging. *Nat. Nanotechnol.* **4**, 710 (2009).

10. Hong, G. *et al.* Multifunctional in vivo vascular imaging using near-infrared II fluorescence. *Nat. Med.* **18**, 1841 (2012).
11. Hong, G. *et al.* Through-skull fluorescence imaging of the brain in a new near-infrared window. *Nat. Photonics* **8**, 723 (2014).
12. Bruns, O. T. *et al.* Next-generation in vivo optical imaging with short-wave infrared quantum dots. *Nat. Biomed. Eng.* **1**, 0056 (2017).
13. Hong, G. & Dai, H. In Vivo Fluorescence Imaging in the Second Near-Infrared Window Using Carbon Nanotubes. in *In Vivo Fluorescence Imaging: Methods and Protocols* (ed. Bai, M.) 167–181 (Springer New York, 2016). doi:10.1007/978-1-4939-3721-9_15
14. Welsher, K., Sherlock, S. P. & Dai, H. Deep-tissue anatomical imaging of mice using carbon nanotube fluorophores in the second near-infrared window. *Proc. Natl. Acad. Sci.* **108**, 8943 (2011).
15. Carr, J. A. *et al.* Shortwave infrared fluorescence imaging with the clinically approved near-infrared dye indocyanine green. *Proc. Natl. Acad. Sci.* (2018). doi:10.1073/pnas.1718917115
16. Chen, Y. *et al.* Shortwave Infrared in Vivo Imaging with Gold Nanoclusters. *Nano Lett.* **17**, 6330–6334 (2017).
17. Franke, D. *et al.* Continuous injection synthesis of indium arsenide quantum dots emissive in the short-wavelength infrared. *Nat. Commun.* **7**, 12749 (2016).

Appendix

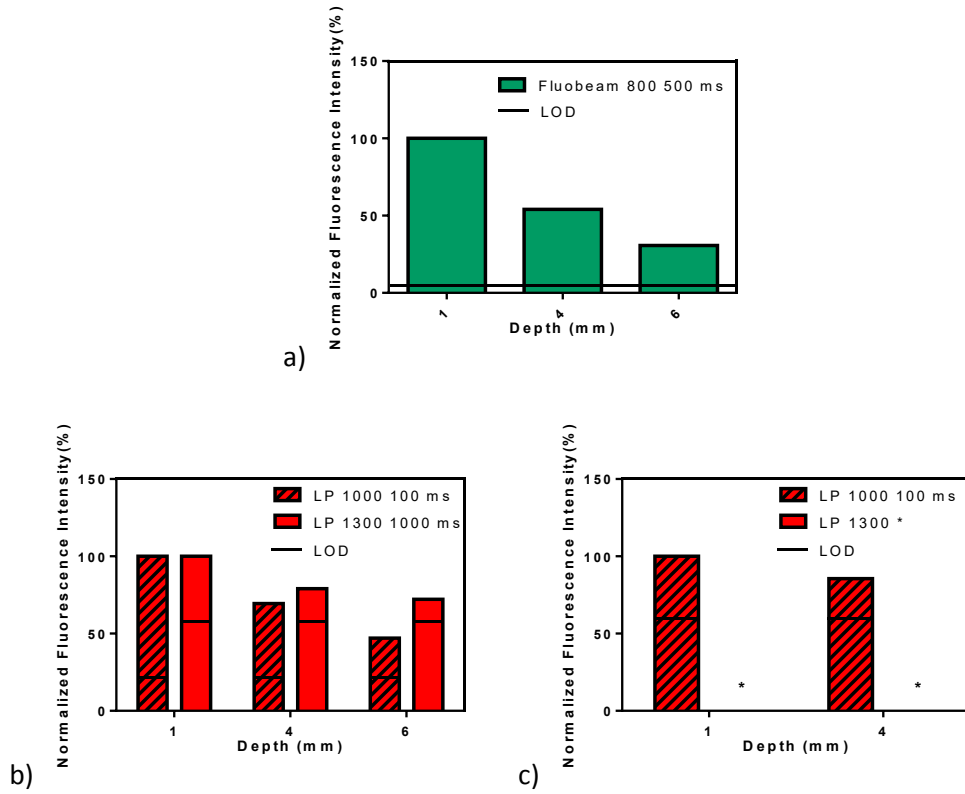


Figure 34. Normalized fluorescence intensity of ICG versus depth: a) Fluobeam®800, λ_{exc} 780 nm, 500 ms exposure time for LP 830 nm, b) SWIR platform, λ_{exc} 720 nm, 100 ms exposure time for LP 1000 nm, 1s exposure time for LP 1300 nm, c) SWIR platform, λ_{exc} 810 nm, 100 ms exposure time for LP 1000 nm, not detectable (*) for LP 1300 nm.

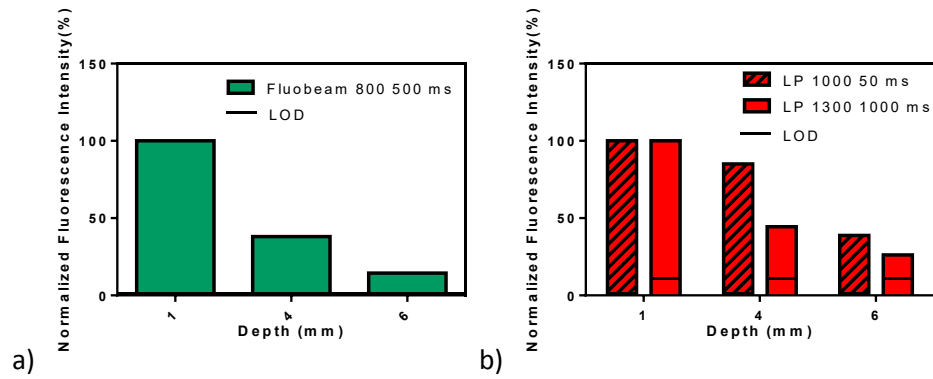


Figure 35. Normalized fluorescence intensity of IR 800 versus depth: a) Fluobeam®800, λ_{exc} 780 nm, 5 ms exposure time for LP 830 nm, b) SWIR platform, λ_{exc} 720 nm, 50 ms exposure time for LP 1000 nm, 1s exposure time for LP 1300 nm.

Assembly and calibration of bioimaging SWIR platform

Master thesis

Trainee : Benjamin HOUANG

19/02/2018

Table of contents

I.	Connections' verification.....	4
a.	Princeton camera: NIRvana™ 640 ST	4
b.	Excitation ring.....	5
c.	Optical bench (lens + emission filters)	7
II.	Operation	8
a.	Lightfield software.....	8
b.	Gardasoft controller	18

I. Connections' verification

a. Princeton camera: NIRvana™ 640 ST

1. Camera's power supply



2. Ethernet connection to computer



3. Set the height of the camera at your discretion. First before turning the wheel at the top of the column, make sure the optical bench is unlocked (the second tape mark starting from the bottom on the column might provide enough space to work under the light ring without diminishing to much the excitation power arriving on the work plan).



b. Excitation ring

1. Gardasoft controller power supply



2. Gardasoft controller/computer connection

3. Gardasoft controller/LEDs connection : check white wire is plugged on the +



- 4.** 8 LEDs' connections (Be careful there are notches on the connections see the red arrow)



- 5.** Set the position of the ring with respect to the camera using the inverted knob (DO NOT exceed the upper limit set by the tape on the side of the screwing axis → you might damage the LEDs connections while tilting them).



- 6.** Switch ON the LEDs at the desired wavelength (see section II.b.).
- 7.** Overlap the four light disks thanks to the dedicated tilting screws on the top part of the ring in order to get the most homogeneous excitation (use the power meter to check along the cross-section and the periphery).



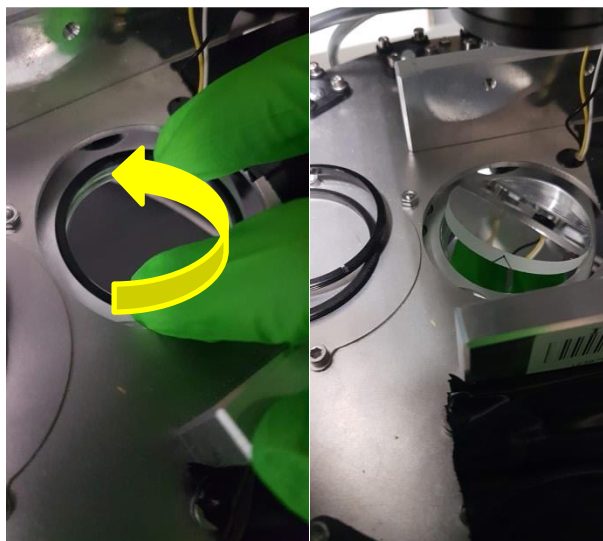
c. Optical bench (lens + emission filters)

There are three lenses (12.5 mm, 25 mm, 50 mm; Navitar) and three Long Pass filters (LP 850 nm, LP 1000 nm, LP 1300 nm; Edmund Optics) available.

1. Screw the Navitar lens on the C-mount adapter of the camera.



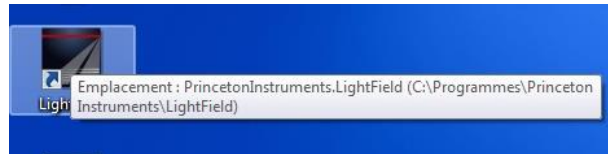
2. Place the Long Pass filters on the dedicated wheel: the reflective coating of the filter must be on the upper side (the arrow on the side of the filter must be up).



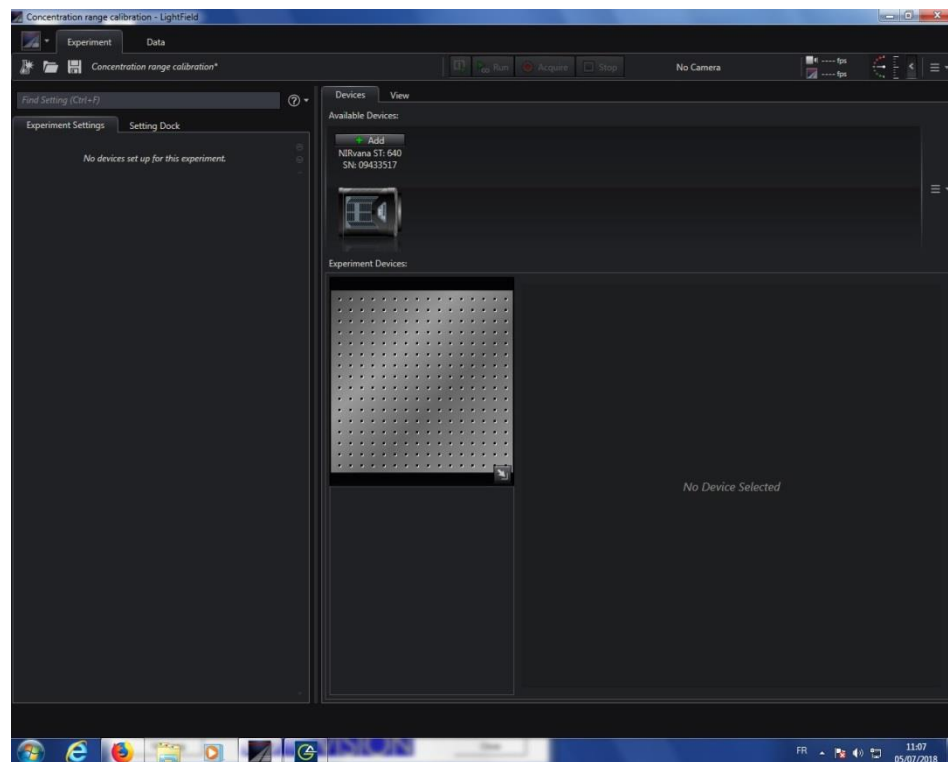
II. Operation

a. Lightfield software

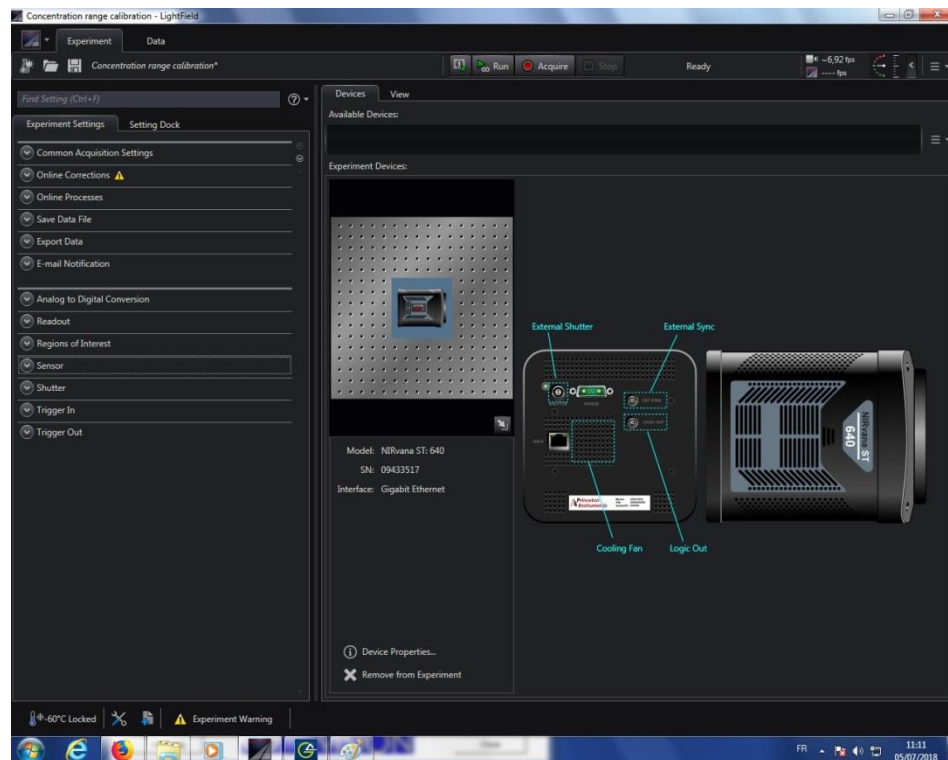
1. Switch ON the camera.
2. Launch the Lightfield interface.



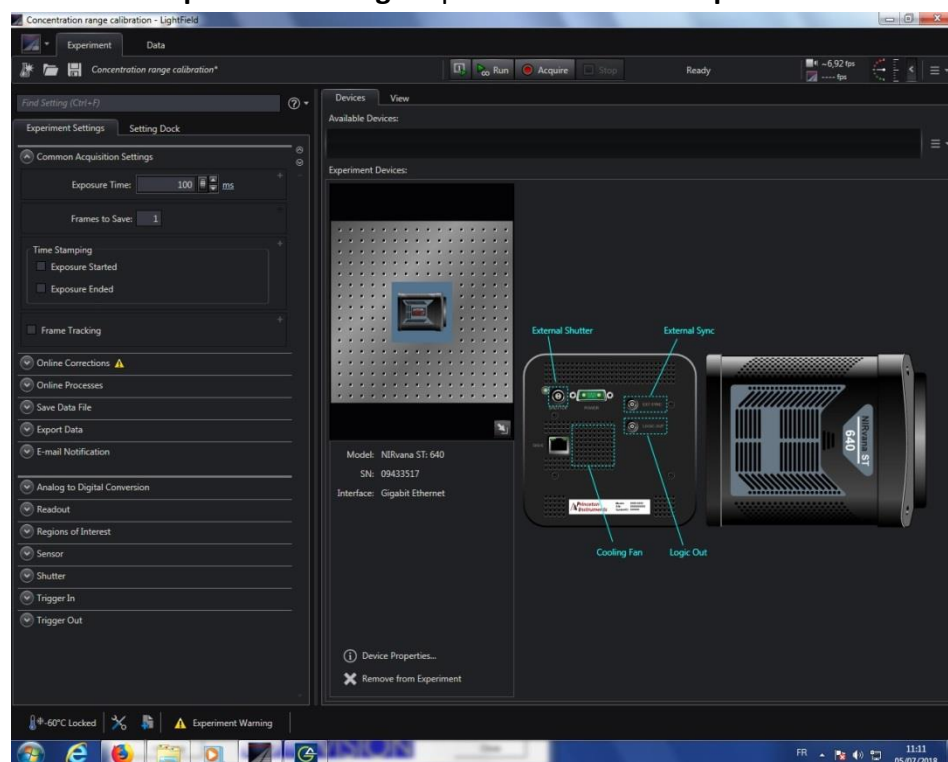
3. Select the **Devices** tab of the **Experiment** workspace and wait until the icons are loaded into the **Available Devices** area.



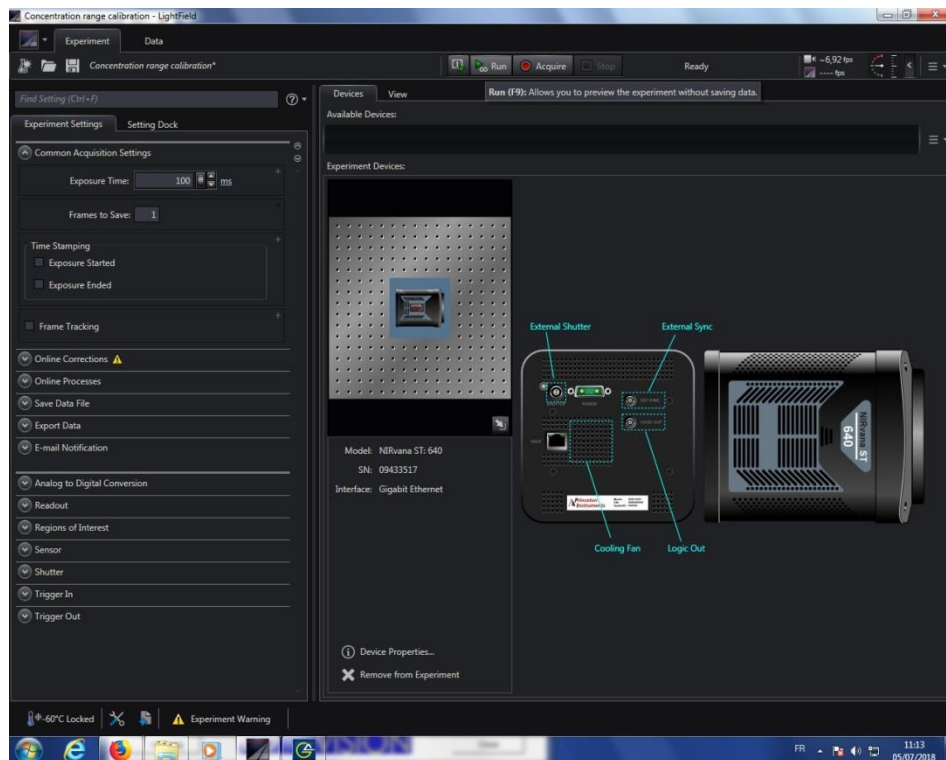
4. Drag these icons into the **Experiment Devices** if they are not already in. The appropriate expenders should appear in the **Experiment Settings** stack on the left side of the window.



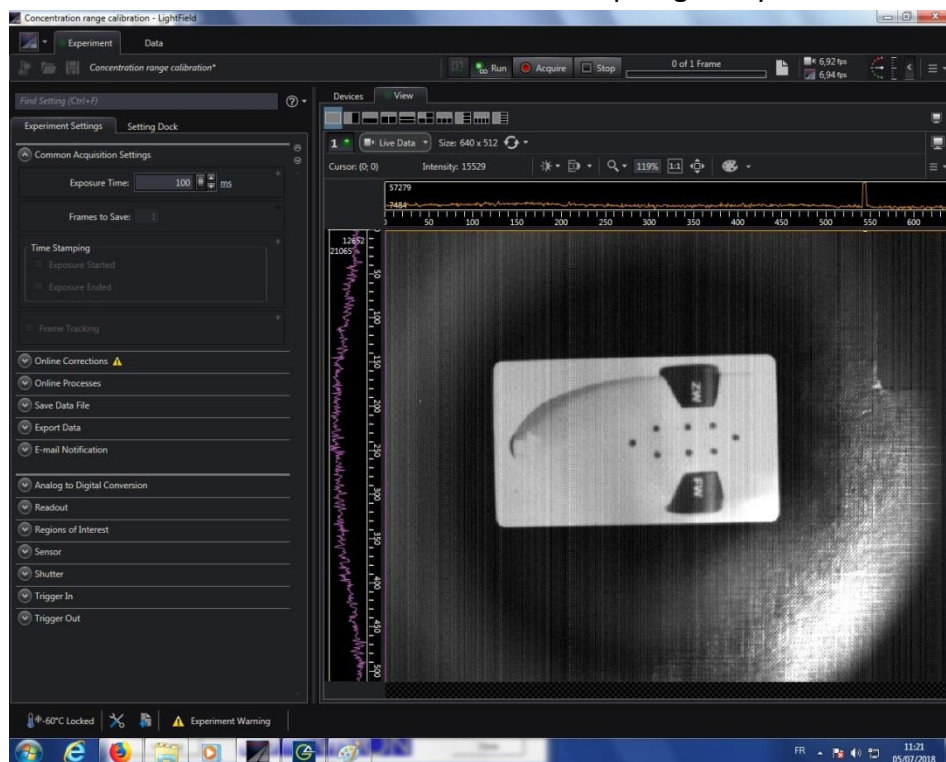
5. In the **Common Acquisition Settings** expander enters the **Exposure time**.



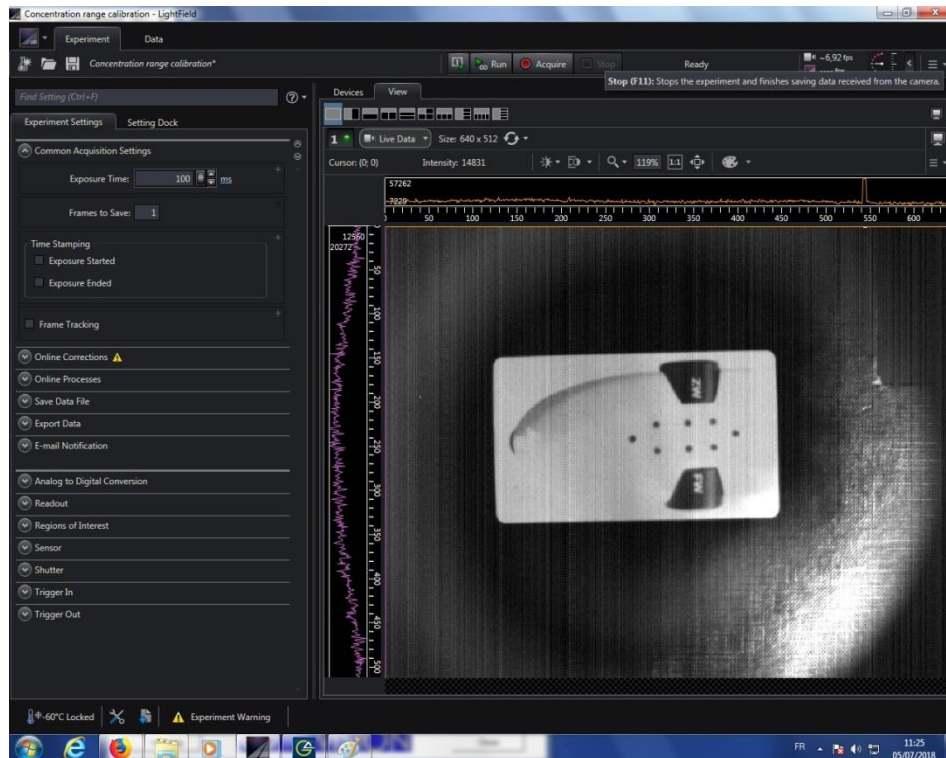
6. Click **Run** at the top of the window.



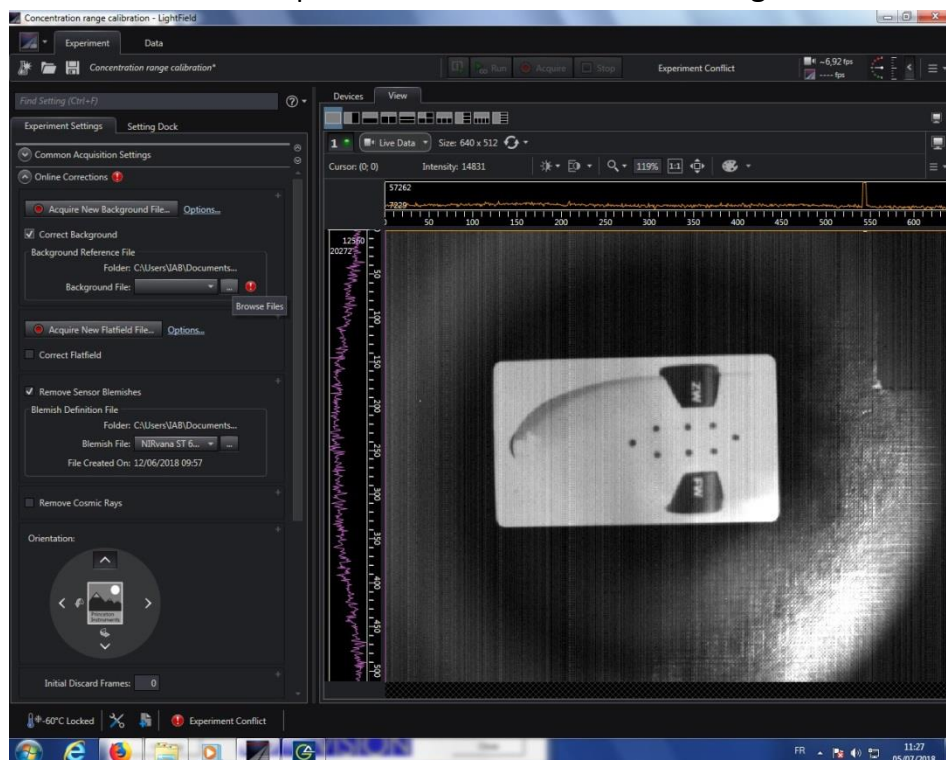
7. Make sure the Navitar lens is in focus and set the diaphragm at your discretion.



8. Click **Stop** at the top of the window.

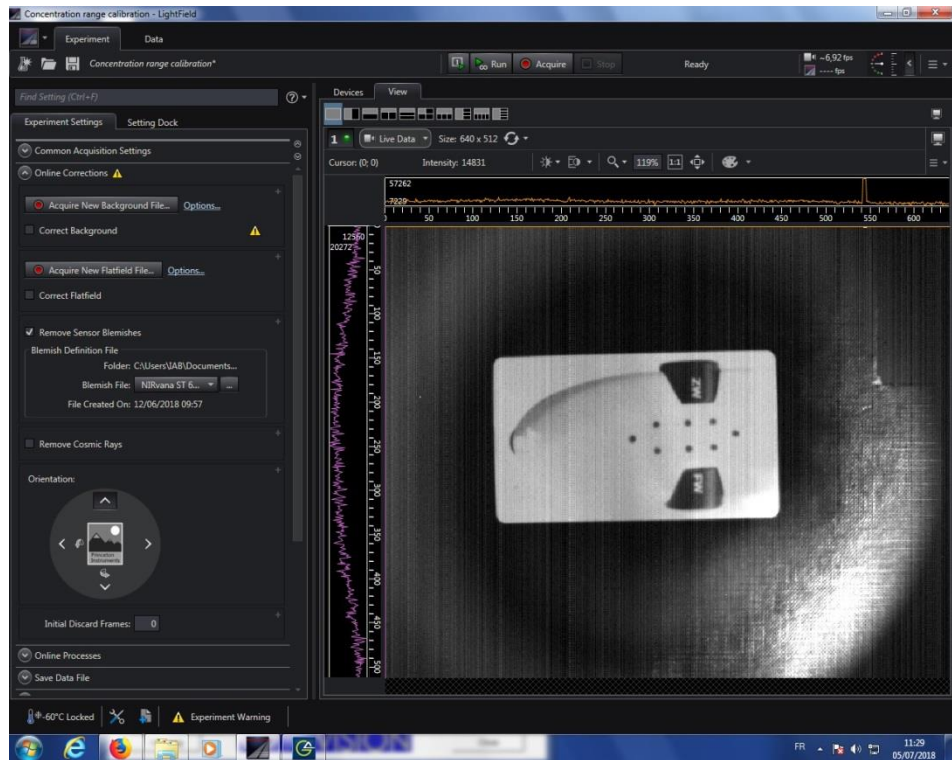


9. In the **Online Corrections** expander check the box **Correct Background**.

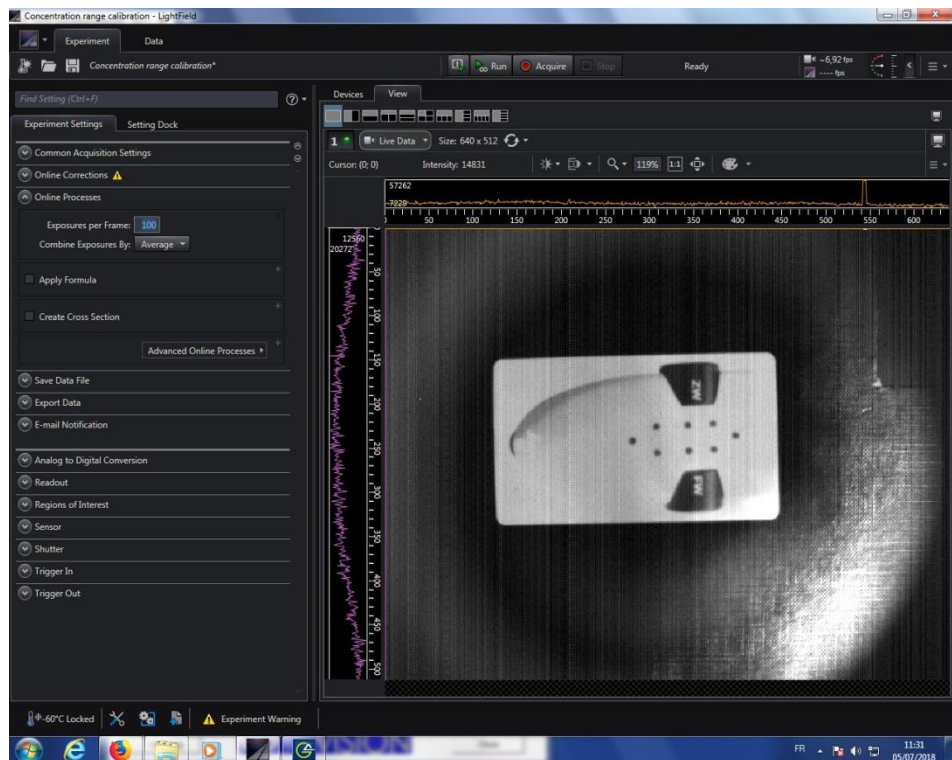


10. If the appropriate background (taken in the appropriate conditions: exposure time, filter) is available in the folder *Mes Documents* → *Lightfield* → *Correction files* jump to the step 11. If not, you have to take it by the following procedure:

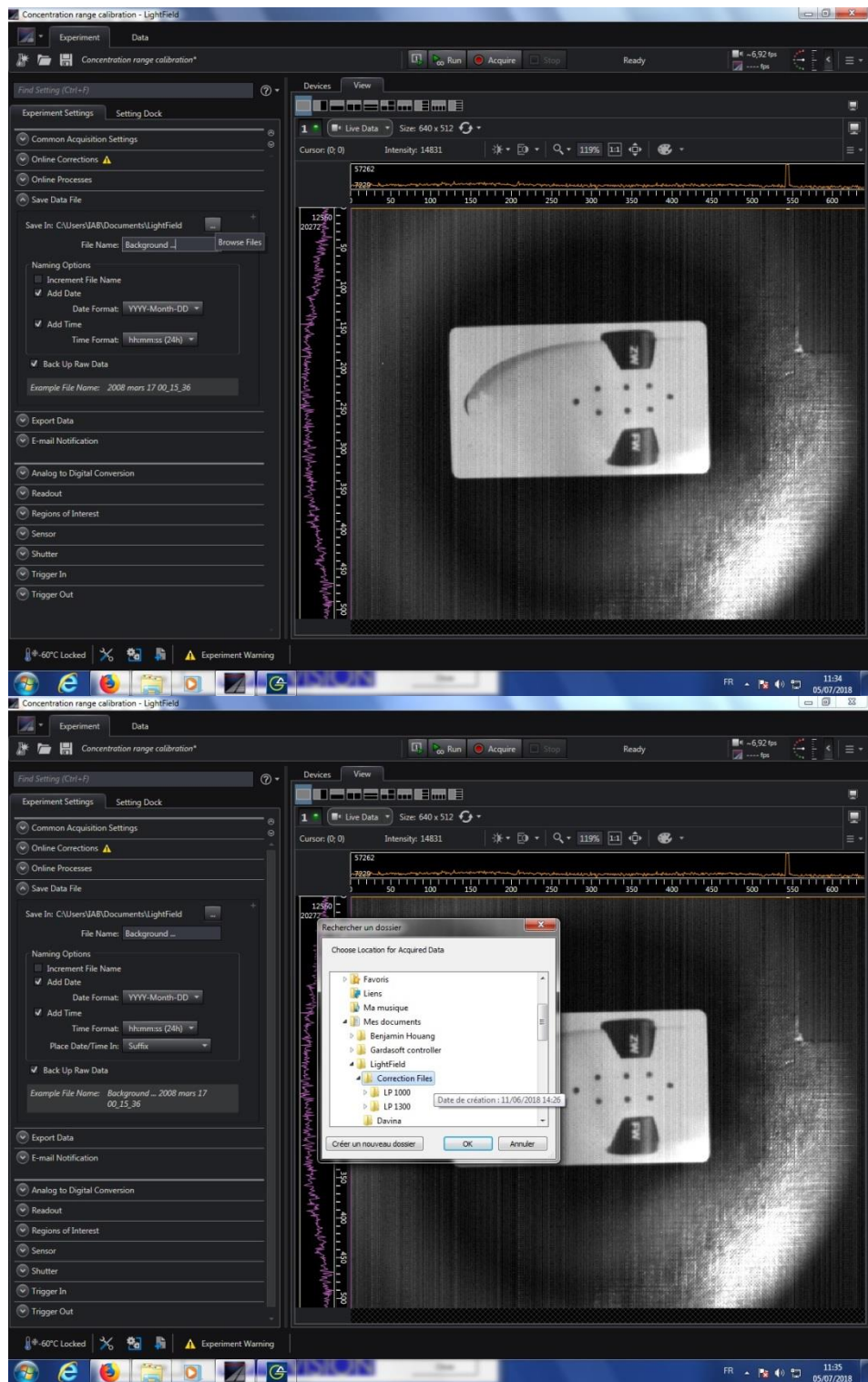
- i. Uncheck the box **Correct Background**.



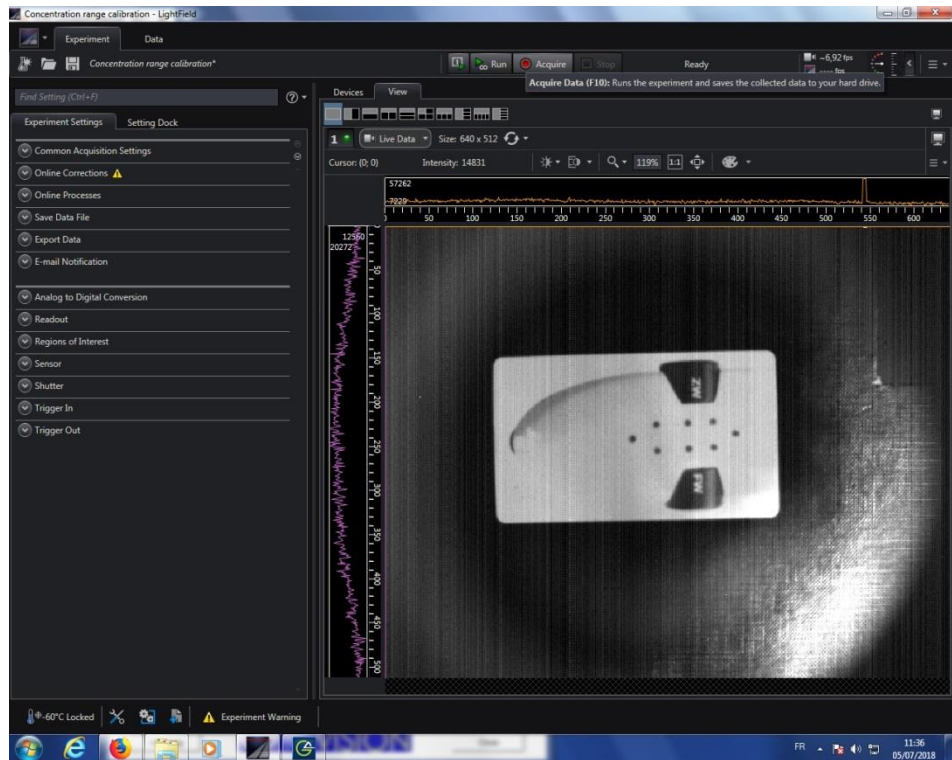
- ii. In the **Online Process** expander enter **100 Exposure per frame** and select **average**.



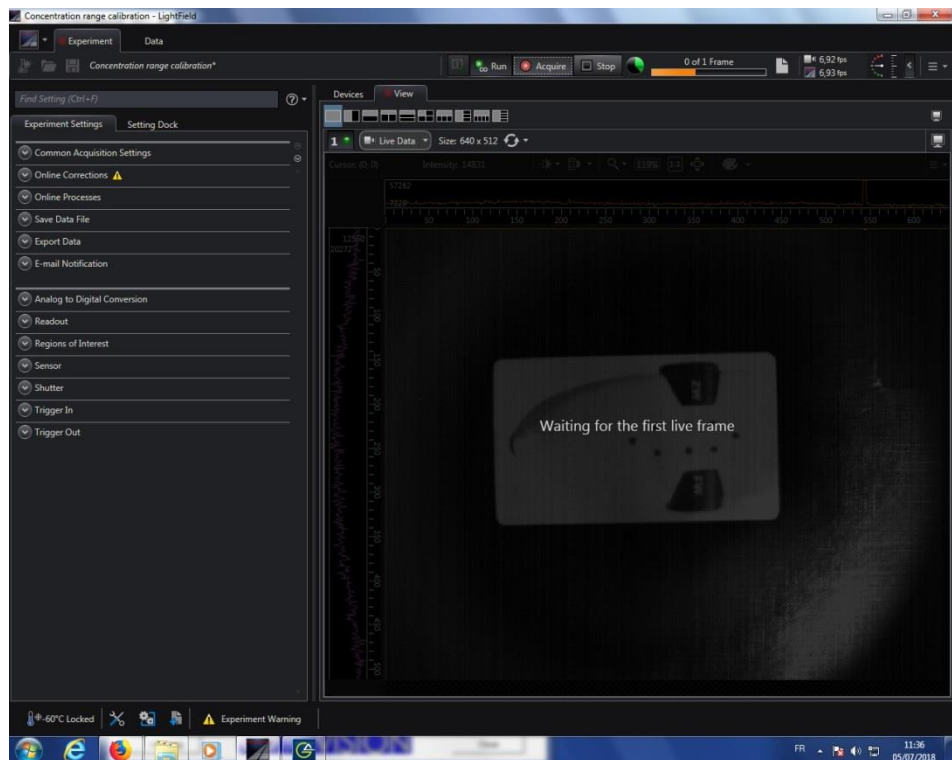
- iii. In the **Save Data file** expander select the *Correction files* folder and give a name to your future background.

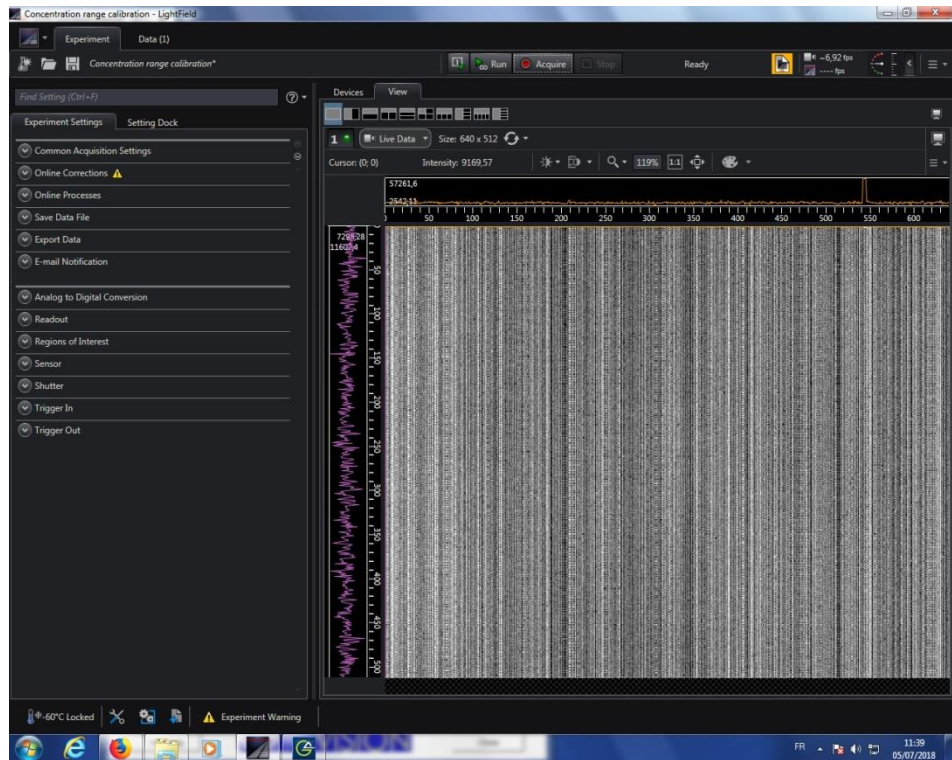


iv. Click **Acquire** at the top of the window.

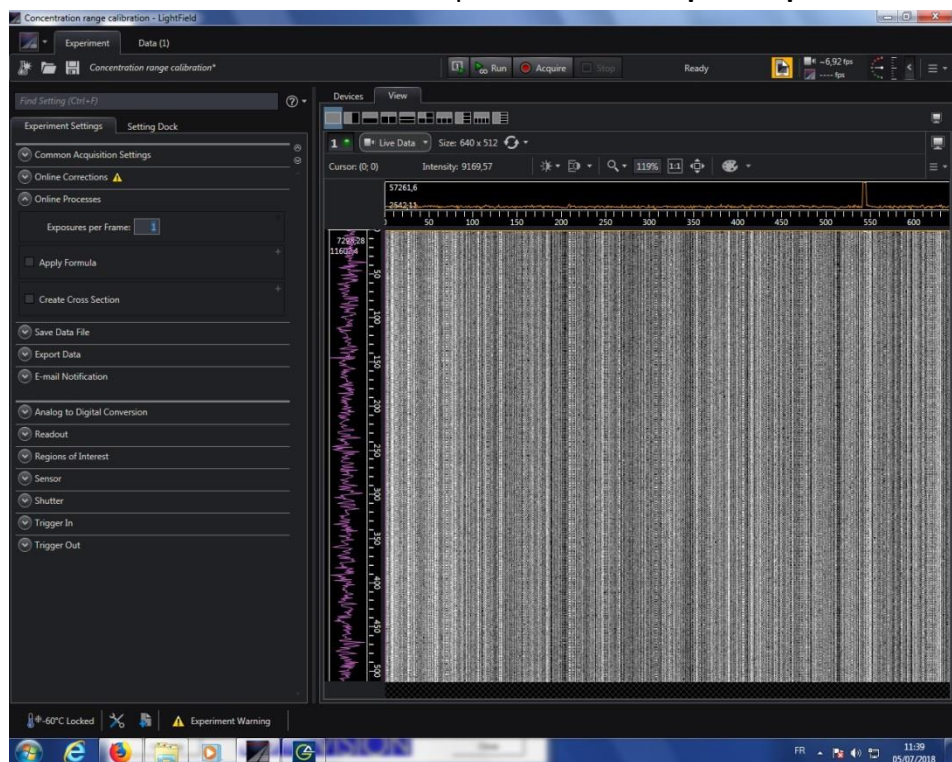


- v. Wait until acquisition is over by checking the loading bar at the top of the screen.

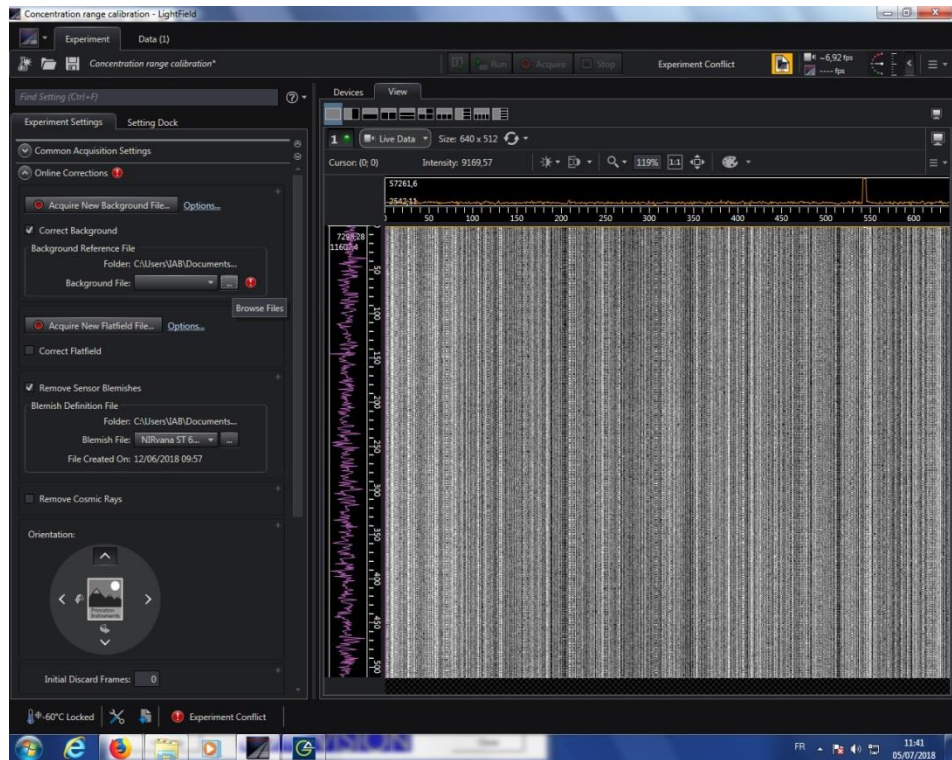




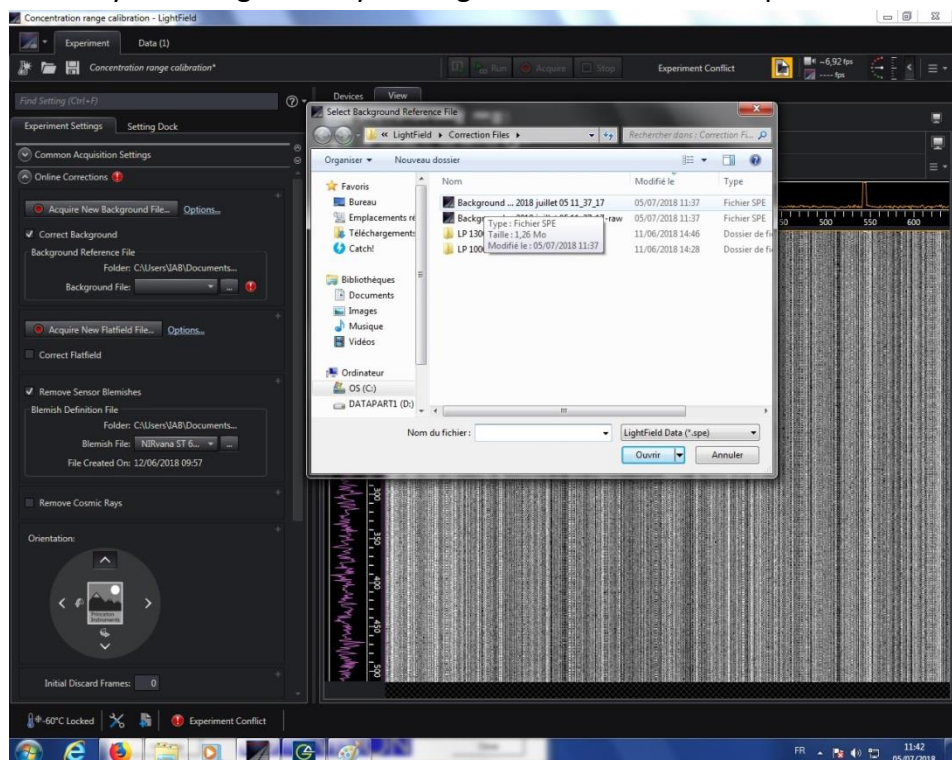
vi. Go back to the **Online Process** expender enter **1 Exposure per frame**.



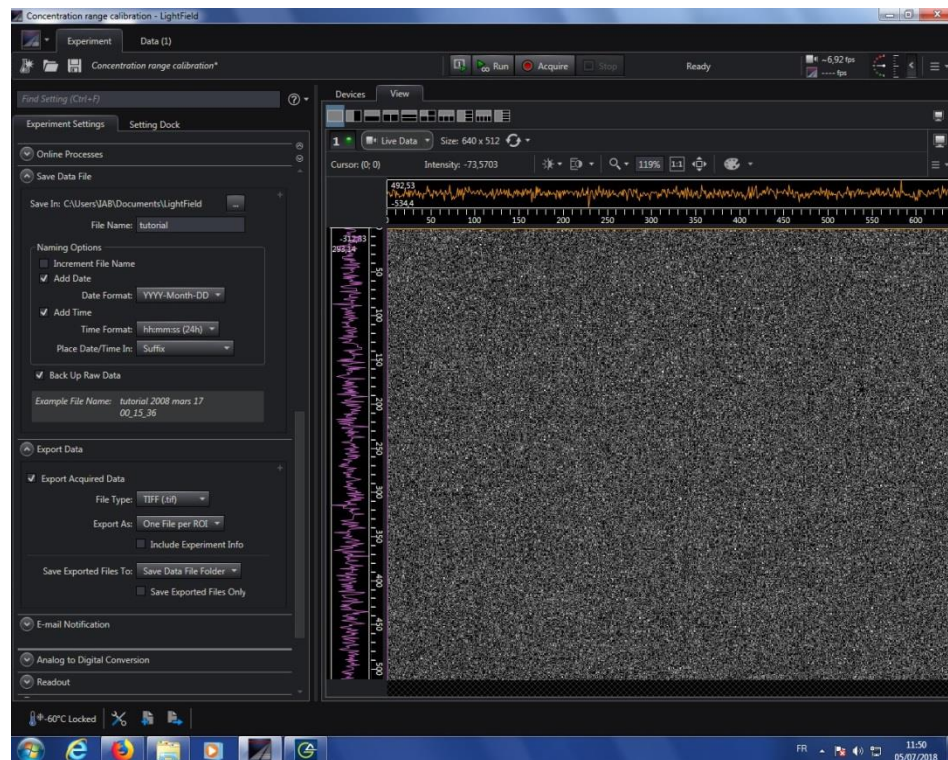
vii. In the **Online Corrections** expender check the box **Correct Background**.



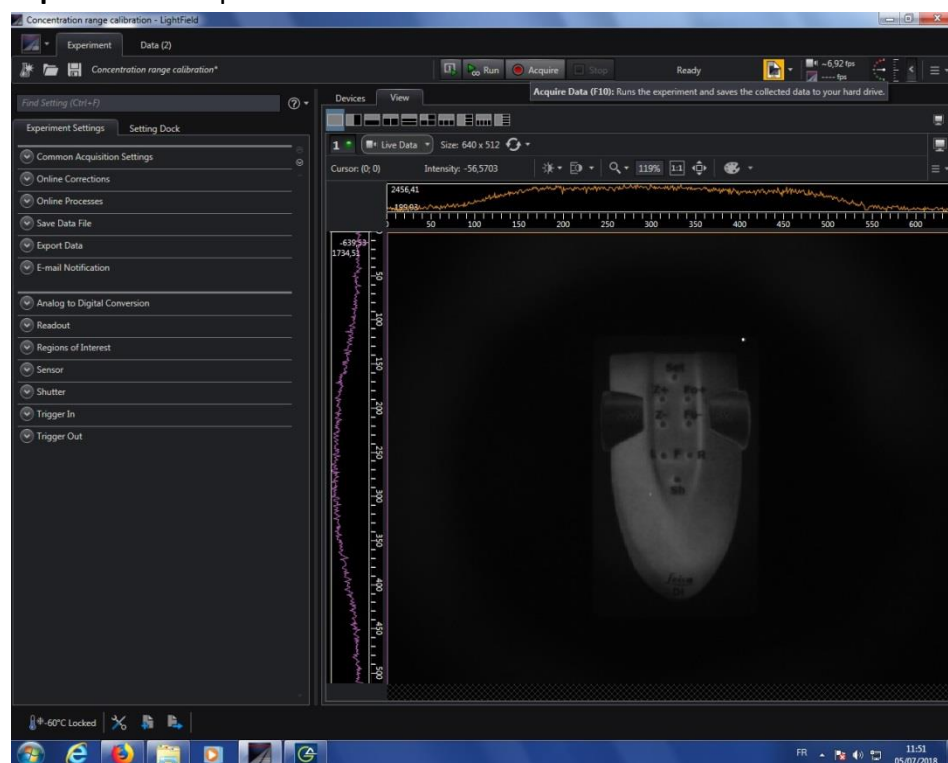
viii. Select your background by clicking on the Browse files' square.



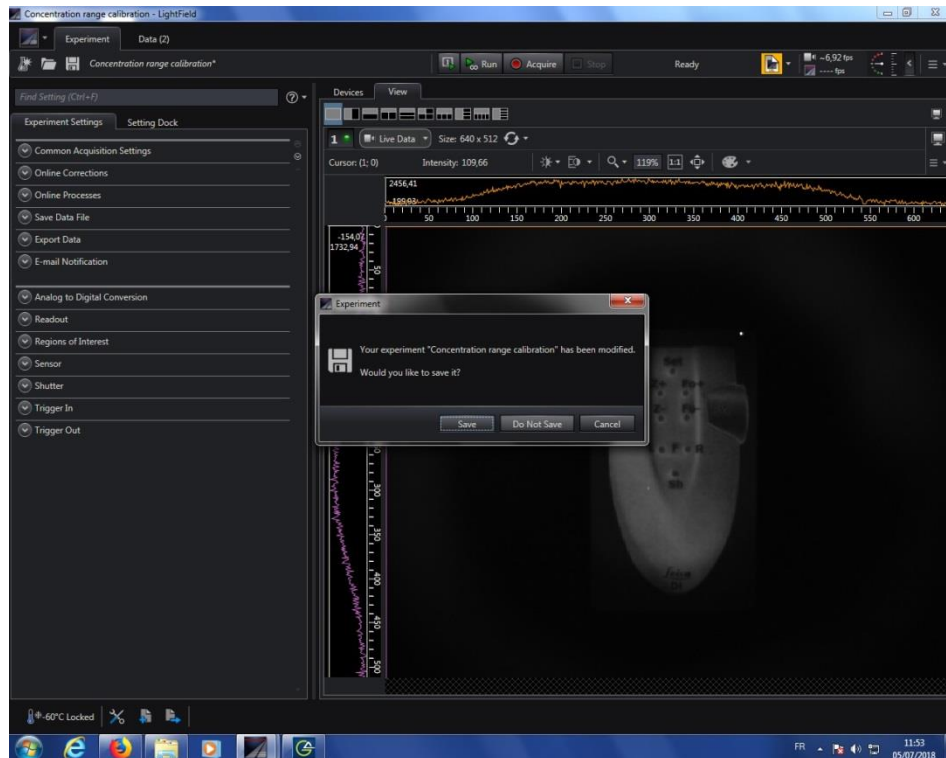
11. Change the settings in the **Save Data** file and **Export Data** file expanders at your discretion.



12. Turn ON the LEDs (see next chapter).
13. Place your sample under the light ring.
14. Click **Acquire** at the top of the window.



15. When experiments are finished, close the Lightfield software before switching OFF the camera. You can save your experiment settings at your discretion.

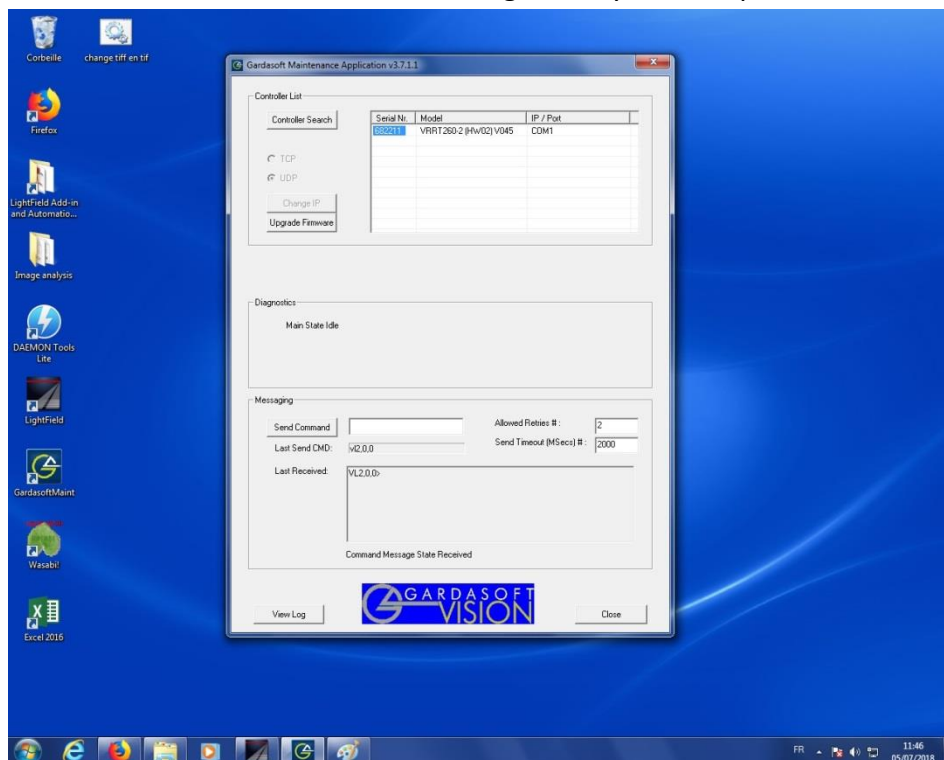


b. Gardasoft controller

1. Open the Gardasoft interface.



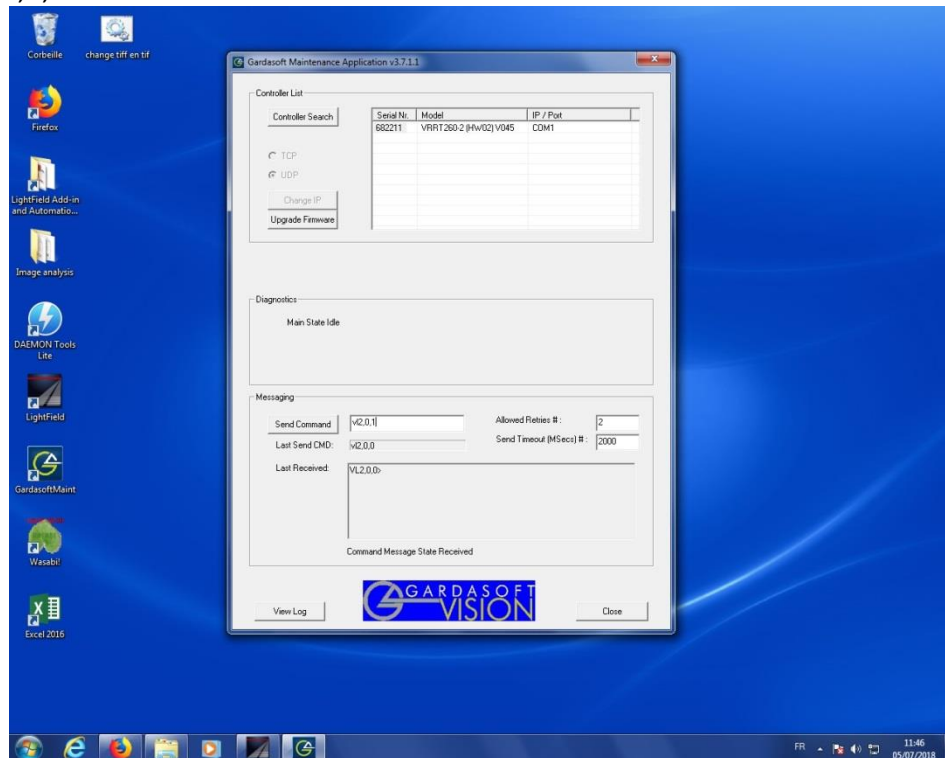
2. In the first window select the controller recognized by the computer.



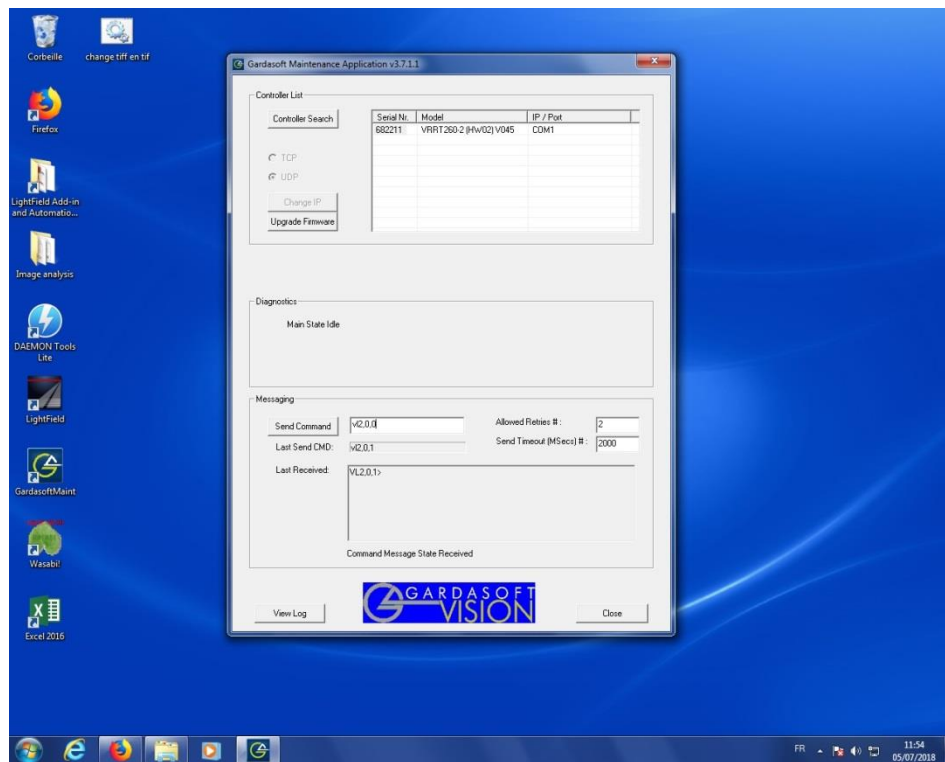
3. In command line enter the current in the following way:

VL channel (1 for the 810 nm, 2 for the 720 nm), **0**, **current value in A** (do not exceed 1 A)

Ex: VL2,0,1



4. Press enter.
5. To set the brightness of the LEDs type:
RS channel, percentage of brightness
Ex: RS2,100
6. Press enter.
7. When you are done with your experiments, do not forget to turn OFF the LEDs.



Abstracts

Recently, the near-infrared spectral window known as SWIR for ShortWave InfraRed or NIR II between 850 and 1700 nm was investigated by several research groups for bioimaging. Despite the development of cameras in this spectral window for military, industrial or artistic applications, their use for biomedical applications remains scarcely exploited. The SWIR window has the advantage of a fall in photon scattering and tissue autofluorescence compared to Vis-NIR I domains. This internship focused on the assembly and first calibration of SWIR imaging platform based at the Institute IAB in Grenoble. Several types of SWIR probes have been tested in intralipid phantoms, under chicken slices and *in vivo* in mice. It highlighted the importance of getting powerful and homogeneous light source and efficient filtering to obtain high spatial resolution in tissue (up to 4-5 mm).

Récemment, plusieurs groupes de recherche sur la bioimagerie ont étudié la fenêtre spectrale proche infrarouge connue sous le nom de SWIR pour ShortWave InfraRed ou NIR II entre 850 et 1700 nm. Malgré le développement de caméras dans cette fenêtre spectrale pour des applications militaires, industrielles ou artistiques, leur utilisation pour des applications biomédicales reste peu exploitée. La fenêtre SWIR présente l'avantage de réduire la diffusion des photons et l'autofluorescence des tissus par rapport aux domaines Vis-NIR I. Ce stage a porté sur l'assemblage et le premier étalonnage de la plateforme d'imagerie SWIR basée à l'Institut IAB de Grenoble. Plusieurs types de sondes SWIR ont été testés sur des fantômes d'intralipide, sous des tranches de poulet et *in vivo* chez la souris. Les résultats ont souligné l'importance d'utiliser une source de lumière puissante et homogène et un filtrage efficace pour obtenir une résolution spatiale élevée dans les tissus (jusqu'à 4-5 mm).

Recentemente, la finestra spettrale del vicino infrarosso nota come SWIR per ShortWave InfraRed o NIR II tra 850 e 1700 nm è stata studiata da diversi gruppi di ricerca per la bioimaging. Nonostante lo sviluppo di telecamere in questa finestra spettrale per applicazioni militari, industriali o artistiche, il loro uso per applicazioni biomediche rimane scarsamente sfruttato. La finestra SWIR ha il vantaggio di una diminuzione della diffusione dei fotoni e dell'autofluorescenza dei tessuti rispetto ai domini Vis-NIR I. Questo stage si è concentrato sull'assemblaggio e la prima calibrazione della piattaforma di imaging SWIR con sede presso l'Istituto IAB di Grenoble. Diversi tipi di sonde SWIR sono stati testati su intralipidi, sotto fette di pollo e *in vivo*. Ha evidenziato l'importanza di ottenere una sorgente di luce potente e omogenea e un filtraggio efficiente per ottenere un'elevata risoluzione spaziale nei tessuti (fino a 4-5 mm).